Appendix 5C-3: Evaluation of Phosphorus Sources, Forms, Flux, and Transformation Processes in the Stormwater Treatment Areas

Odi Villapando and Jill King

INTRODUCTION

The overarching goal of the Evaluation of Phosphorus Sources, Forms, Flux, and Transformation Processes in the Stormwater Treatment Areas (P Flux Study) is to enhance the understanding of the mechanisms and factors that affect phosphorus (P) treatment performance of stormwater treatment areas (STAs), particularly those that are key performance drivers at the lower reaches of the treatment trains. In order to gain this understanding, it is critical to evaluate the P sources, forms, flux, and transformation processes along the STA flow-ways (FWs). The information would provide the basis for development or enhancement of strategies that could improve the capabilities of the STAs to meet the water quality based effluent limits (WQBELs). The study was designed to address two key Restoration Strategies Science Plan for the Everglades Stormwater Treatment Areas (Science Plan; SFWMD 2013) questions:

- How can internal loading of P to the water column be reduced or controlled, especially in the lower reaches of the treatment trains?
- How can the biogeochemical or physical mechanisms be managed to further reduce soluble reactive phosphorus (SRP), particulate phosphorus (PP), and dissolved organic phosphorus (DOP) concentrations in the outflow of the STAs?

The study consists of several components and substudies: (1) data mining, (2) organic P speciation, (3) FW assessments at different flow conditions, (4) in situ particle dynamics, (5) in situ P flux measurements, (6) soil characterization, (7) assessment of enzyme and microbial activity, (8) vegetation assessments, and (9) quantification of faunal role in P cycling. In addition, limited data are being collected at Water Conservation Area (WCA) 2A for comparison purposes. These substudies are in various stages of implementation. Once completed, using conceptual models as a guide, both new and existing STA information will be analyzed, synthesized, and integrated using both the top-down and the bottom-up approaches. The top-down approach will employ data mining techniques to identify master variables in the low P domain (Figure 1). The bottom-up approach will focus on developing and improving mathematical equations to characterize the relationship among the different boxes and drivers ("arrows") in order to predict the various P fluxes and pools in the conceptual model (Figure 2).

Preliminary results from the following substudies are presented in this report:

- FW Water Quality Assessments
- P Flux Measurements

- Spatial Patterns of Soil P Concentrations and Storages
- Effects of Faunal Communities on Water Quality

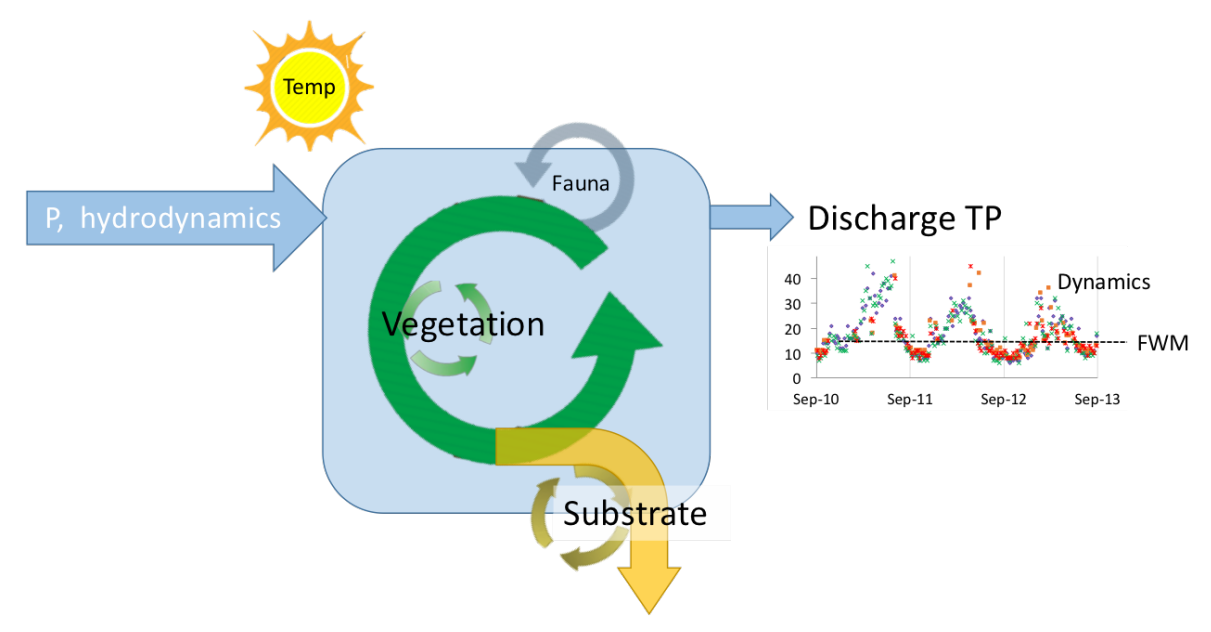


Figure 1. Top-down factors for consideration in P Flux Project data integration. Circular arrows suggest P turnover rates within various compartments, including, for example, both slow (e.g. aquatic macrophyte) and fast (e.g. epiphyte, phytoplankton, etc.) compartments associated with vegetation. The "hydrodynamics" category includes factors such as water velocity, residence time and depth. (Note: FWM – Flow-weighted Mean, Sep – September, and TP – total phosphorus.)

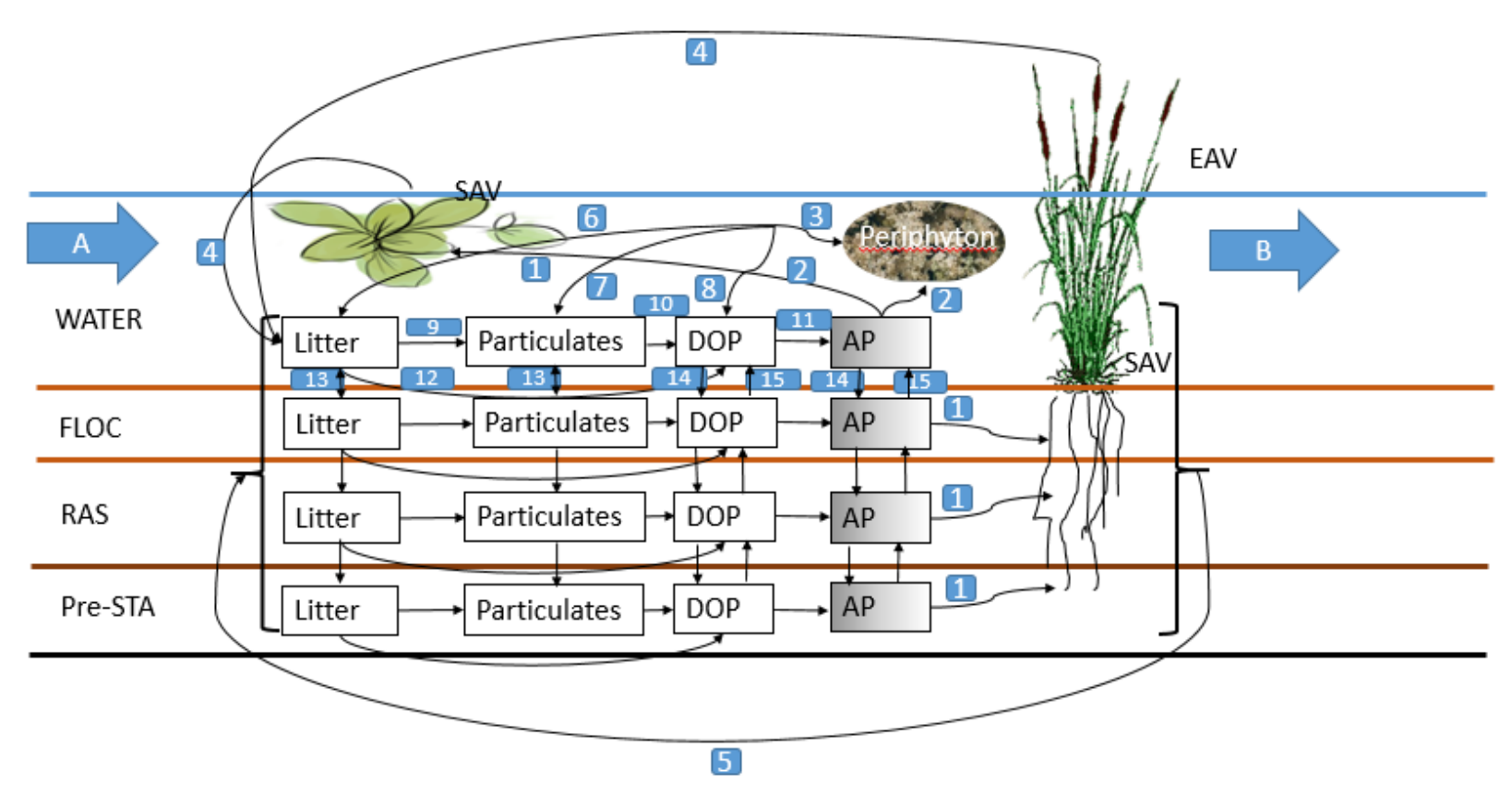


Figure 2. Conceptual model with state variables and fluxes to be incorporated into a numerical framework. The figure depicts a length segment within an STA cell. The state variables are operating in 4 domains, which are water, floc, active, and pre-STA soil. Carbon and P will be tracked in all the pools containing organic forms of P, which include the emergent aquatic vegetation (EAV), submerged aquatic vegetation (SAV), periphyton, litter, particulates, dissolved organic phosphorus (DOP). The thick arrows (A and B) indicate import and export of P into and out from the depicted length segment, respectively. The thin arrows represent P (and to some degree carbon) fluxes. The numbers identify the respective flux, which include (1) uptake of available P (AP) by EAV and SAV plants, (2) P uptake by periphyton from the water domain, (3) incorporation of plant and other organic materials into periphyton, (4) litterfall and plant mortality, (5) root mortality, (6, 7, 8) disintegration of periphyton, (9) litter fragmentation, (10) decomposition of organic matter, (11) mineralization of organic matter (12) leaching from litter, (13) sedimentation and resuspension of litter and particulate (fragmented) organic matter, (14) integration of available P into floc, active and stable domain via evaporation pumping, and (15) diffusion of AP across domains. The gradient fill for AP includes the partitioning of DOP into sorbed and desorbed species, where the sorption potential changes across the domain.

FLOW-WAY WATER QUALITY ASSESSMENTS

Odi Villapando, Jill King, Rupesh K. Bhomia¹, and Paul Julian, II¹

INTRODUCTION

This field study is part of an evaluation of the biogeochemical responses of the different regions along the selected STA FWs to three different flow scenarios: stagnant, low flow, and high flow. The objective is to obtain quantitative and qualitative information on nutrient dynamics in the water column during different flow conditions that will be used to determine the factors influencing the measured biogeochemical responses and their relative magnitudes, particularly those related to P sources, P flux, and P species transformations.

METHODS

The STA FWs chosen for this study were STA-2 FW 1, STA-2 FW 3, and STA-3/4 FW 3 (Cells 3A and 3B). These specific FWs were selected to represent good performing FWs (those that have achieved outflow TP concentration of 20 micrograms per liter $[\mu g/L]$ or lower), and represent different FW configurations, vegetation communities, and soil conditions. The results presented here are from the three controlled flow events conducted in STA-2 FW 3 between February and November 2016. This is a single cell FW with predominantly submerged aquatic vegetation (SAV) and a large patch of emergent aquatic vegetation (EAV) in the eastern region of the FW (**Figure 3**). The pre-STA soil in the FW is highly organic but the current soil profile consists of predominantly inorganic floc material on top of recently accreted soil, and the pre-STA soil underneath the recently accreted soil. The outflow flow-weighted mean TP concentration for this FW for the entire period of record, Water Year 2002 (WY2002; May 1, 2001–April 30, 2002) to WY2016, is 18 μ g/L.

The first flow event was conducted from February 22 to April 11, 2016, for a period of 50 days. This event consisted of a high flow period (February 22–March 7), followed by a stagnant (no inflow) period (March 8–29), and then a normal post-stagnant operational period (March 30–April 11) (**Table 1**). Normal post-stagnant operation refers to the period when the FW was returned to routine operation without any targeted flow rates. During the 14-day high flow period, the average flow was 325 cubic feet per second (cfs) and the resulting P loading rate was 3.7 milligrams P per square meter per day (mg P/m²/d) or 1.35 grams P per square meter per year (g P/m²/yr). There were no flows into the FW during the 23-day period of stagnation and the outflow gate was closed. During the post-stagnant period, the FW received an average flow of 55 cfs and 1.0 mg P/m²/d (0.36 g P/m²/yr).

The second flow event was conducted from June 27 to August 29, 2016, for a period of 64 days (**Table 1**). This flow event was preceded by a stagnant period of over three months due to restrictions associated with migratory bird nesting. Samples were collected, and field measurements were conducted during a 6-day period without inflow, representing the conditions during this long period of stagnation, then over three weeks of low flow (average 132 cfs), from July 3 to July 24. The FW was kept under stagnant condition for two weeks from July 25 to August 8, and transitioned back into low flow (average 120 cfs), from August 9 to August 29. P loadings during the first and second low flow periods were 1.6 mg P/m²/d (0.58 g P/m²/yr) and 2.3 mg/m²/d (0.84 g/m²/yr), respectively.

¹University of Florida, Gainesville, Florida.

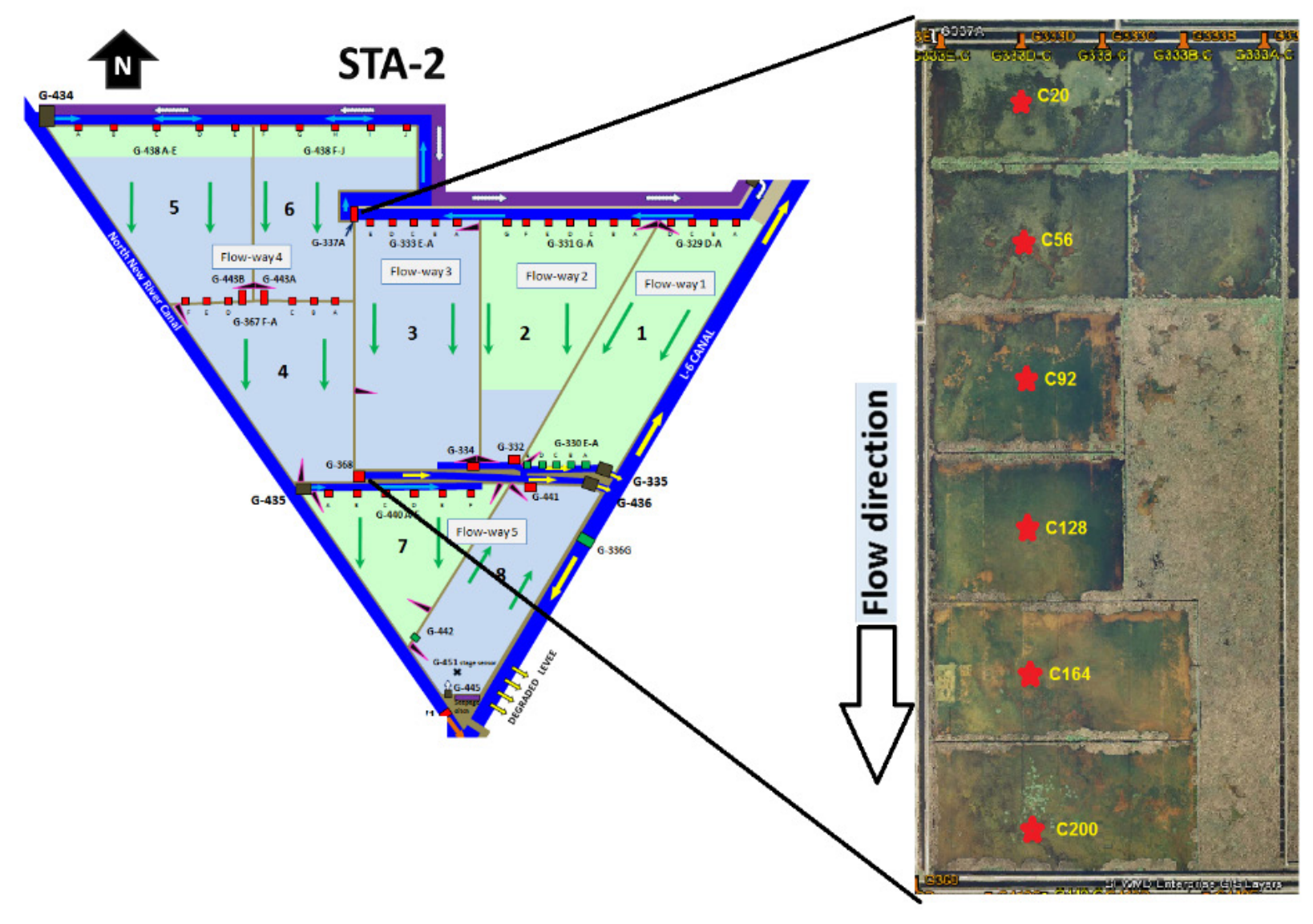


Figure 3. STA-2 FW 3 map showing the water quality monitoring stations.

Table 1. Hydrologic conditions and hydraulic loading rate (HLR), and phosphorus loading rate (PLR) during the flow events. Values for water depth, flow, HLR, and PLR are averaged over phase period ± standard deviation. ^a

Phase Period		Water Depth (ft)	Flow (cfs)	HLR (cm/d)	PLR (mg/m²/d)					
	1 st Flow Event (February 22–April 11, 2016) – 50 days									
High Flow	2/22 – 3/7	1.96 ± 0.04	325 ± 60	8.55 ± 1.58	3.7 ± 1.3					
Stagnant	3/8 – 3/29	1.91 ± 0.06	0	0	0					
Post-stagnant	3/30 – 4/11	1.60 ± 0.21	55 ± 111	1.45 ± 2.91	1.0 ± 2.0					
	2 nd Flow E	Event (June 27–Aug	vent (June 27-August 29, 2016) - 64 days							
Stagnant	6/27 – 7/2	1.46 ± 0.05	0	0	0					
Low Flow	7/3 – 7/24	2.03 ± 0.18	132 ± 33	3.48 ± 0.87	1.6 ± 0.7					
Stagnant	7/25 – 8/8	1.93 ± 0.07	0	0	0					
Low Flow	8/9 – 8/29	2.00 ± 0.07	120 ± 86	3.15 ± 2.26	2.3 ± 1.6					
3 rd Flow Event (October 12–November 22, 2016) – 42 days										
High Flow	10/22 – 11/3	2.46 ± 0.14	300 ± 51	7.90 ± 1.34	5.9 ± 2.1					
Stagnant	11/4 – 11/22	2.32 ± 0.10	0	0	0					

a. Key to units: cfs – cubic feet per second; cm/d – centimeters per day; ft – feet; and mg/m²/d – milligrams per square meter per day.

The third flow event was conducted from October 12 to November 22, 2016, for a 42-day period (**Table 1**). This event consisted of a three-week high flow period from October 12 to November 3, followed by a three-week period of stagnation (no inflow) from November 4 to November 22. During the high flow period, the FW received an average flow of 300 cfs and 5.9 mg P/m²/d (2.15 g P/m²/yr).

Continuous monitoring of water quality and field conditions during the flow events was conducted at six water quality monitoring stations along the inflow to outflow transect of the treatment FW (Figure 3). The stations were equipped with autosamplers, EXO-sondes, water level loggers, and HOBO light meters. The autosamplers collected six water samples daily at four-hour intervals (0200, 0600, 1000, 1400, 1800, and 2200), which were analyzed for total phosphorus (TP) on discrete samples and total nitrogen (TN) and total organic carbon (TOC) on daily composited samples. Weekly surface grab samples were also collected from these sites and analyzed for TP, soluble reactive P (SRP), total dissolved P (TDP), dissolved organic carbon (DOC), TN, calcium (Ca), magnesium (Mg), potassium (K), sodium (Na), ammonium (NH₄⁺), nitrogen oxides (NO_x), iron (Fe), sulfate (SO₄²-), chloride (Cl), aluminum (Al), alkalinity, color, total suspended solids (TSS), hardness, and chlorophyll. In situ measurements of pH, temperature, specific conductance, and dissolved oxygen (DO) at 15-minute intervals were collected using EXO-sondes. Particulate P (PP) was calculated as the difference between TP and TDP, and DOP was calculated as the difference between TDP and SRP. Phosphorus speciation data were obtained from weekly grab samples due to limitations with pre-preservation of auto sample containers. The use of sulfuric acid to preserve auto samples can promote hydrolysis of labile organic P and condensed inorganic P, resulting in an overestimation of SRP and underestimation of DOP. Collection of high resolution data, both spatially and temporally, with the autosamplers allowed the evaluation of diurnal patterns in TP concentrations in the study flow-ways. Key results summarized in the following section provide a comparison of the effects of low and high P loadings on transformations of P in the water column during the stagnant (no flow) condition.

RESULTS

Surface Water TP Concentrations

Autosampler TP data were screened for outliers using a non-parametric approach, in which values greater than the 99th percentile for a given station and flow period were identified as outliers and removed from further statistical analysis (Julian and Hill 2012). One hundred seventeen (117) out of 5,398 data points collected during the three flow events were identified as outliers. Daily mean TP values for each station were calculated and compared between flow periods using Dunn's test, a non-parametric pairwise multiple comparisons procedure based on rank sums following rejection of a Kruskal-Wallis test.

There was a clear TP concentration gradient along the treatment FW at all periods of each of the three flow events (**Figures 4** through **6**). For the first flow event, median inflow to outflow TP concentrations ranged from 39 to 11 µg/L during the high flow period, from 75 to 22 µg/L during the stagnant period, and from 100 to 18 µg/L during the post-stagnant period (**Figure 4**). TP concentrations increased significantly at all stations as the FW transitioned from the high flow to stagnant period. The huge spike in TP concentration at station C20 upon resumption of normal (post-stagnant) operations was the result of moderate to high flows (average 239 cfs) that passed through the FW during the first three days of post-stagnant routine operation. TP concentrations at the lower reaches of the FW were significantly lower than observed during the stagnant condition. Data show a lack of P treatment at station C92, as mean daily TP concentrations at this region of the FW remained high relative to TP concentrations observed at station C56.

The long period of stagnation that preceded the low flow period during the second flow event resulted in TP concentrations higher than those seen during any other period of the flow event (**Figure 5**). Median TP concentrations during the pre-stagnant period were 171 and 58 μ g/L at the inflow (Station C20) and outflow (Station C200) regions of the FW, respectively (**Figure 5**). There was a significant decrease in TP concentrations at all stations as the FW transitioned from the pre-stagnant period to the low flow period. TP concentration reductions from inflow to outflow regions of the FW ranged from 61 to 37%. During the stagnant period following the first low flow period, TP concentrations increased within the inflow and midregions of the FW. At the lower reaches of the FW (Stations C164 and C200), TP concentrations were lower during the stagnant period than during the low flow period. TP concentrations during the second low flow period following the stagnant period tended to decrease at all stations except at the inflow region (C20). As observed during the first flow event, TP concentrations at station C92 remained high and variable across the flow periods, suggesting lack of P treatment and in some cases, higher water column P than at the inflow station.

Consistent with the first flow event, water TP concentrations during the third flow event increased during the stagnant period following a period of high flow (**Figure 6**). The increase was significant especially at the lower regions of the treatment FW. While the spatial pattern in TP concentrations along the treatment FW demonstrates reduction, the elevated TP concentrations at C92 at both periods of the flow event suggest localized internal P loading. A closer evaluation of the soil, vegetation, and microbial data collected at this site will be conducted to determine the P increases observed in this region of the FW.

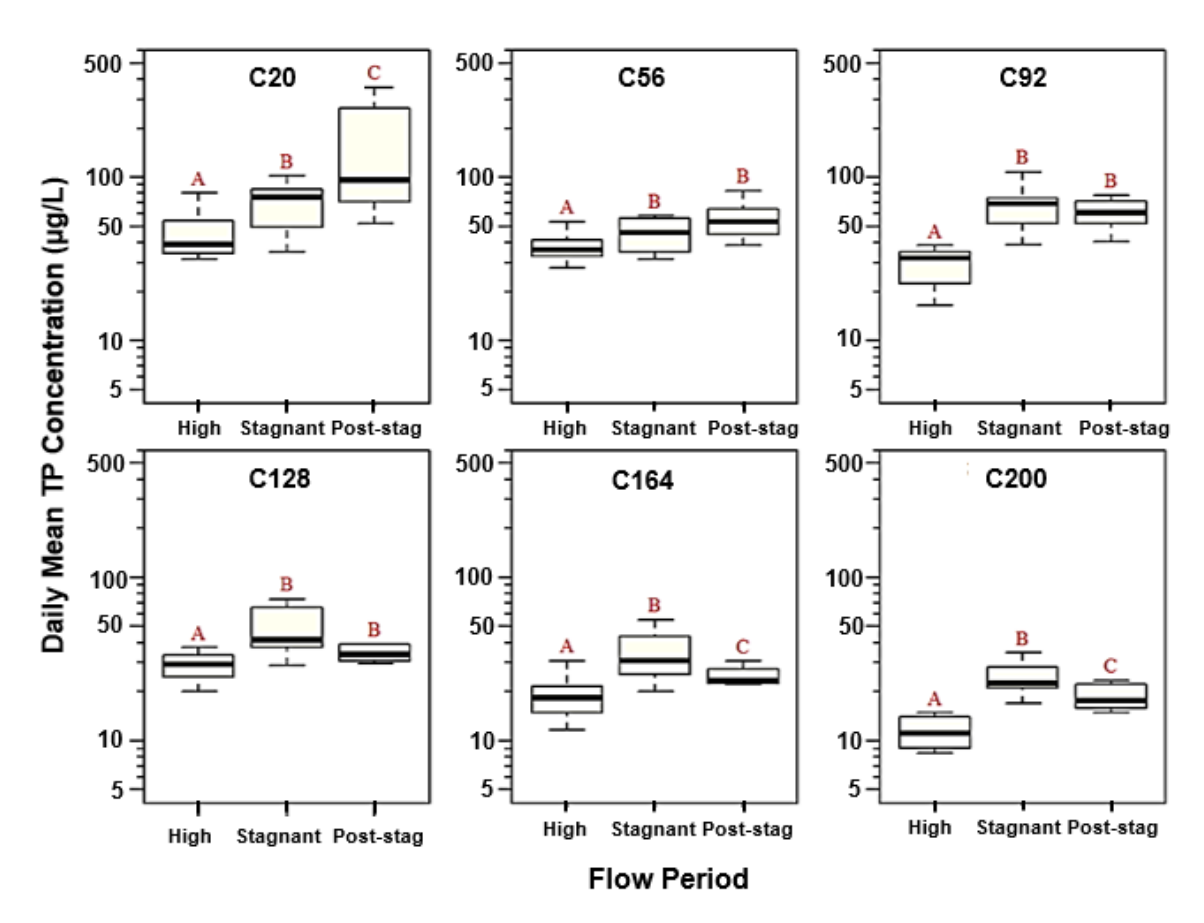


Figure 4. Daily mean TP concentrations in the auto-samples collected every 4 hours at each monitoring station during the first flow event (February 22–April 11, 2016). For a given station, median TP concentrations for any two flow periods with the same letter are not significantly different at a = 0.05 using Dunn's multiple pairwise comparisons. Median TP values are indicated by the band inside the box. Note y-axis is on a log-scale.

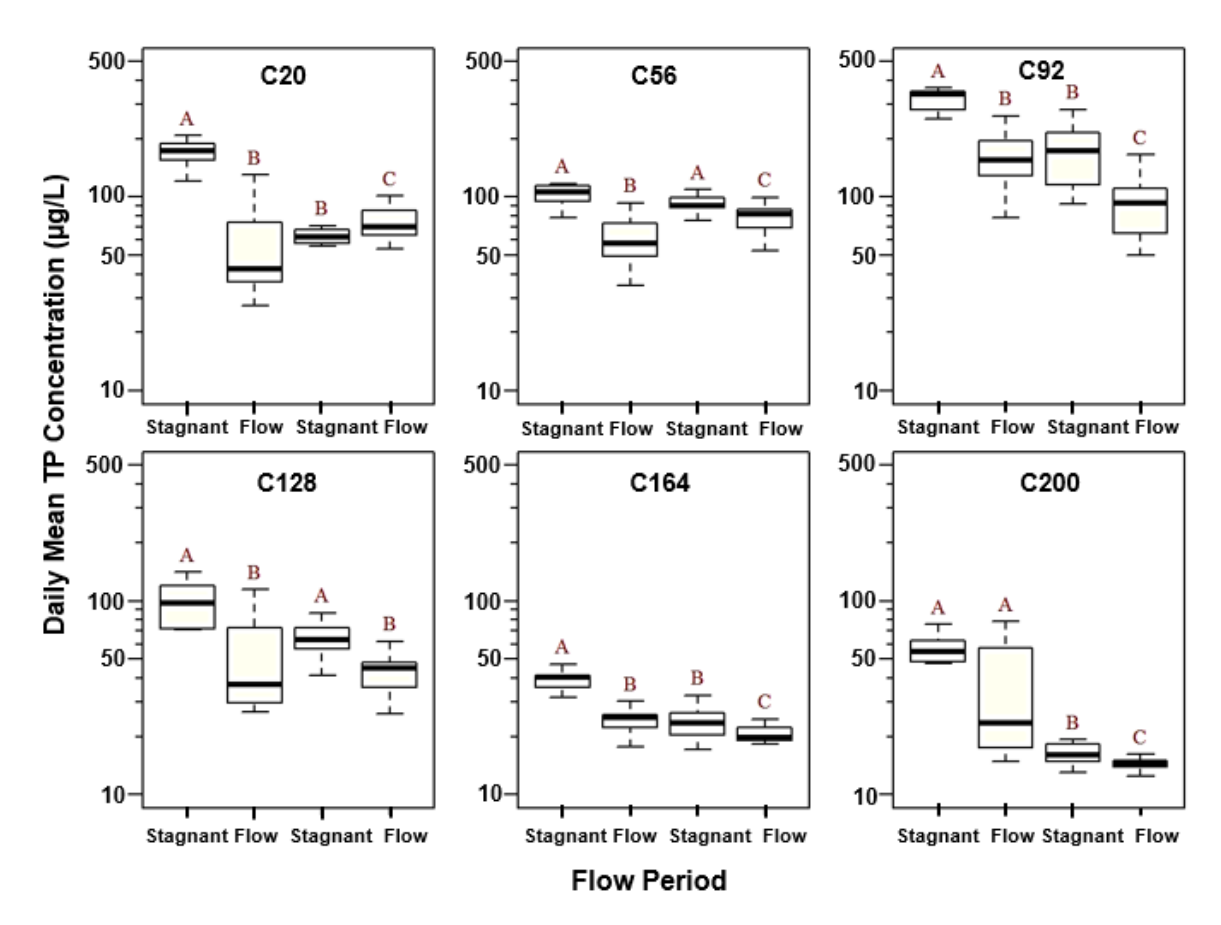


Figure 5. Daily mean TP concentrations in the auto-samples collected every 4 hours at each monitoring station during the second flow event (June 27–August 29, 2016). For a given station, median TP concentrations for any two flow periods with the same letter are not significantly different at a = 0.05 using Dunn's multiple pairwise comparisons. Median TP values are indicated by the band inside the box. Note y-axis is on a log-scale.

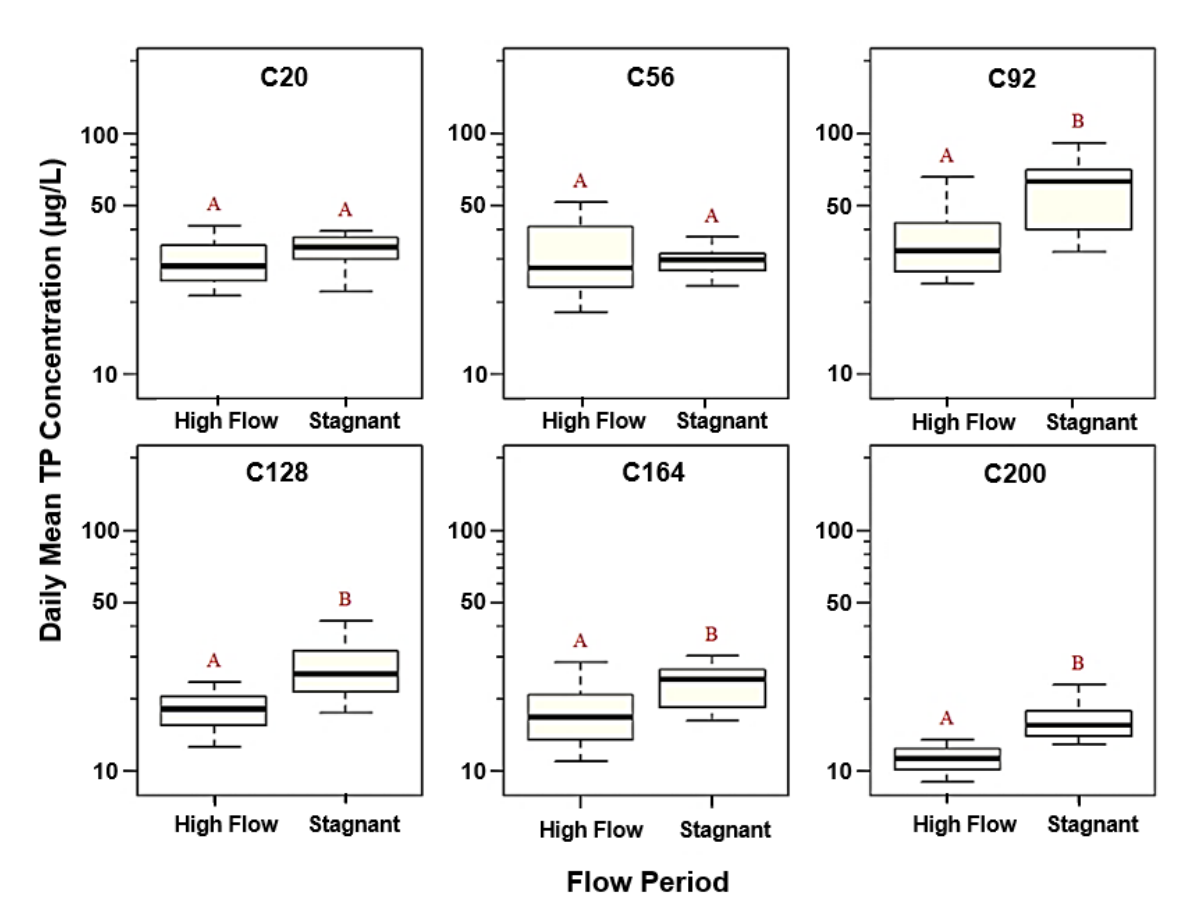


Figure 6. Daily mean TP concentrations in the auto-samples collected every 4 hours at each monitoring station during the third flow event (October 12-November 22, 2016). For a given station, median TP concentrations for the two flow periods with the same letter are not significantly different at $\alpha = 0.05$ using Dunn's multiple pairwise comparisons. Median TP values are indicated by the band inside the box. Note y-axis is on a log-scale.

Patterns in Different P Forms

The different species and concentrations of P in the water column along the transect during the flow event were monitored in weekly grab samples. Consistent with autosampler TP, the weekly grab TP showed P reduction at all periods of each of the three flow events (**Figures 7** through **9**). For the first flow event, mean outflow TP concentrations were 12, 24, and 15 μ g/L at the end of high, stagnant, and post-stagnant flow periods, respectively, for an average concentration reduction of almost 80% (**Figure 7**). Reduction in TP concentration was largely from the reduction in PP, which accounted for 32 to 73% of TP. Both DOP and SRP were also reduced along the FW, but at a more gradual pattern compared to PP, with SRP reduction being steadier and greater than that for DOP. Concentrations of SRP reached minimum detection limit (MDL = 2 μ g/L) starting just past the mid-region of the FW (Station C128) during the entire flow event, indicating that this P form was reduced readily by biotic and abiotic components of the wetland as the water flowed along the FW. Similar to autosampler TP data, the grab TP concentrations during the stagnant period following the high flow period were elevated but started to decline upon resumption of normal post-stagnant flows.

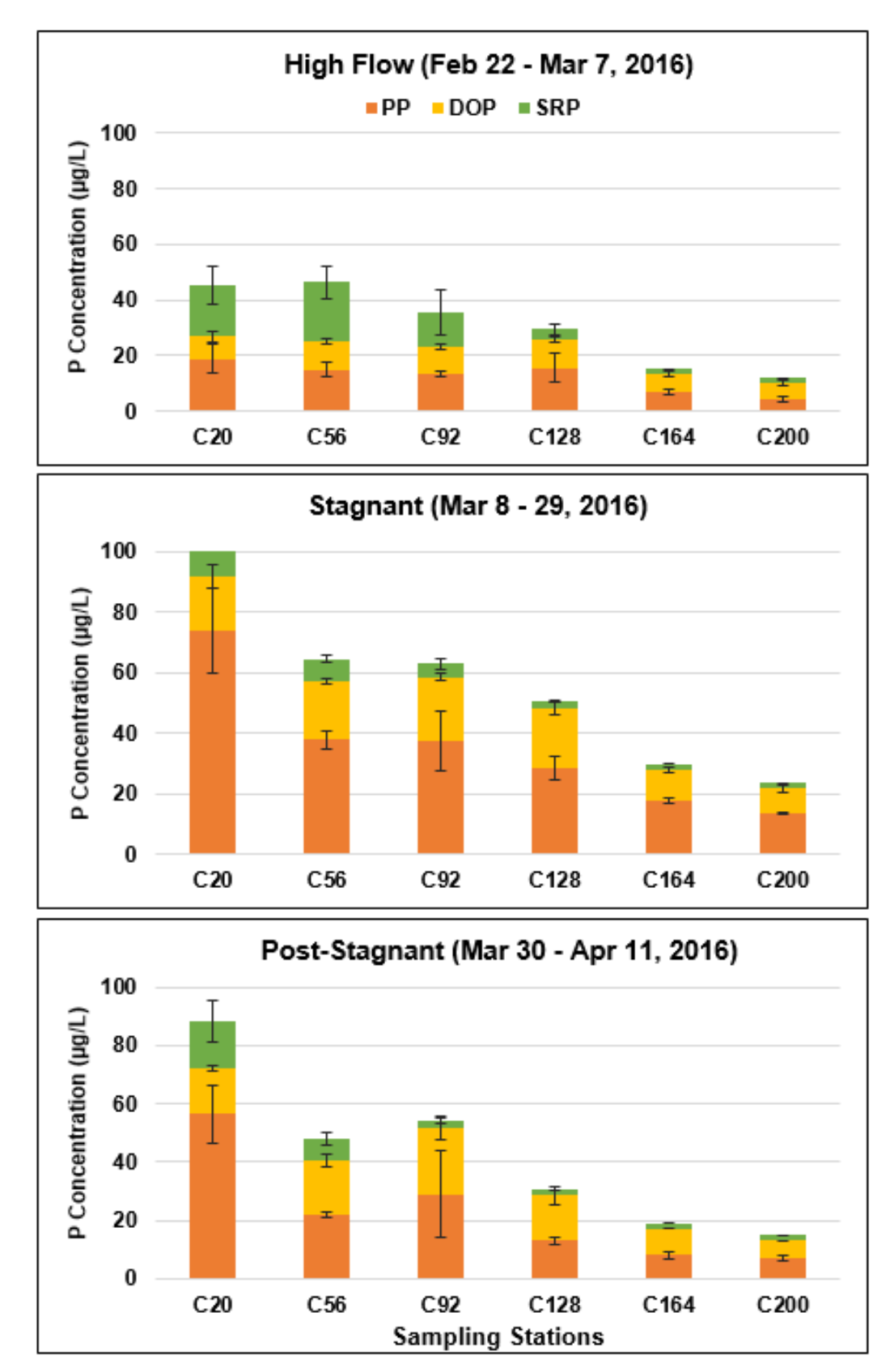


Figure 7. Concentration of the different P forms in the water column along the FW during the first flow event (February 22–April 11, 2016). Error bars represent standard error of the mean.

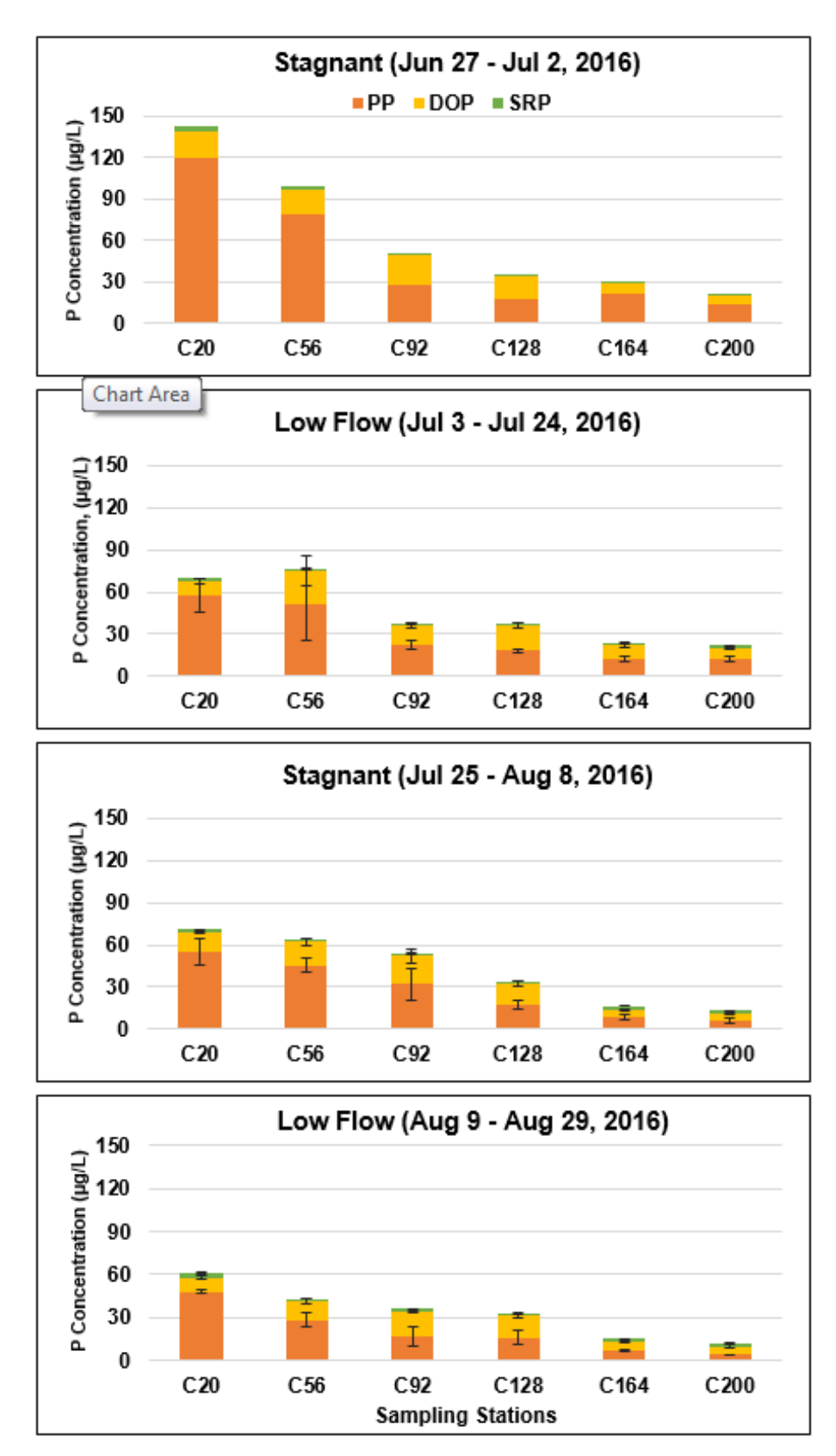
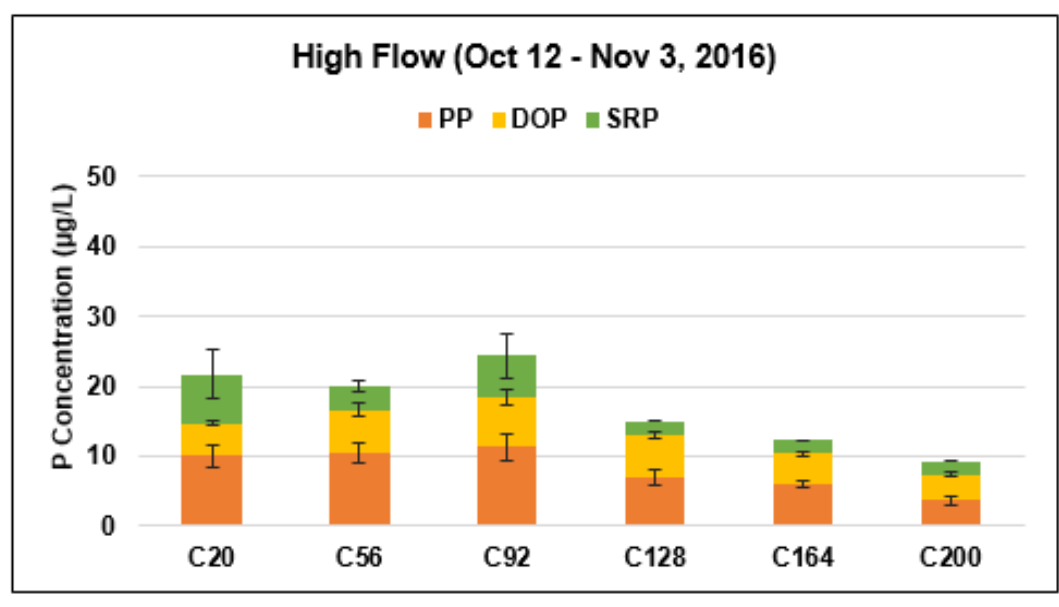


Figure 8. Concentration of the different P forms in the water column along the FW during the second flow event (June 27–August 29, 2016). Error bars represent standard error of the mean.



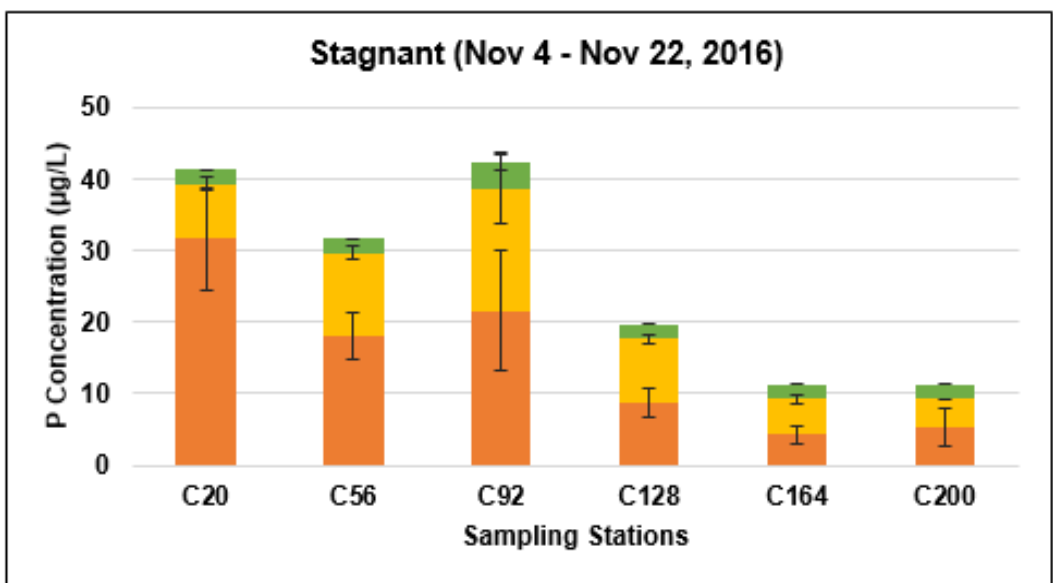


Figure 9. Concentration of the different P forms in the water column along the FW during the third flow event (October 12–November 22, 2016). Error bars represent standard error of the mean.

Despite a spike in TP concentration at Station C92, which was consistent with autosampler TP from all flow events, there was a general reduction trend in TP concentration along the FW during the high flow and stagnant periods of the third flow event (**Figure 9**). Mean TP concentration reductions along the FW were 57 and 73% during the periods of high flow and stagnation, respectively. PP accounted for most of the reduction in TP, especially during the stagnant period when it comprised almost 80% of the TP at the front end of the FW. DOP concentrations were quite variable at or near the inflow region of the FW during the high flow and stagnant periods, with the majority of the reduction occurring at the stations closer to the outflow region of the FW. SRP, which accounted for 32% of the inflow TP, reached MDL ($2 \mu g/L$) at the mid-region of the FW during the high flow period and was at MDL at all regions of the FW (except at Station C92) during the stagnant period. Consistent with the results from the first flow event, TP concentrations were elevated during the stagnant period after a period of high P loading. The increase in TP concentration resulted from a large increase in PP. This indicates that PP is generated in situ, likely

resulting from phytoplankton and microbial growth, and from the formation of amorphous forms of calcium phosphates. PP could also have been produced from senesced SAV or from bioturbation. Additional investigation is needed to determine the magnitude of PP increases from these potential mechanisms.

As with the first flow event, there was a marked reduction in TP concentration along the treatment FW at all periods of the second flow event (**Figure 8**). Mean TP concentrations at the back end of the FW (Station C200) at the end of each of the flow periods were 22, 21, 13, and 12 μ g/L, for an average TP concentration reduction of about 80%. Reduction in PP was the greatest influencer on TP reduction, particularly at the inflow region. DOP also showed reduction along the treatment FW but accounted for only about 13% of TP at the inflow region. SRP was at or near MDL (2 μ g/L) during the entire flow event. The residual P pool at the outflow region of the FW was in the form of PP and DOP. Concentrations of PP were elevated during the pre-stagnant period but were relatively unchanged during the stagnant period following the period of low flow at the stations closer to the inflow and mid regions of the FW.

Correlation of TP with Other Water Quality Parameters

Spearman rank correlation was used to explore empirical relationships between TP and other water quality parameters monitored in weekly grab samples and field measurements taken during the flow events. Correlation analysis was done separately for each of the flow periods (i.e. low flow, high flow, and stagnant) on data pooled from all stations and flow events (**Table 2**). Correlation coefficients indicate the degree and direction of association between two variables but do not imply causality (cause-effect relationship).

Table 2. Spearman rank correlations (Spearman's rho) and probability (p) values between TP and other water quality parameters monitored during the flow events. The signs indicate whether the correlation was positive or negative.

	Low Flow (n = 36) a		High Flow	(n =3 6)	Stagnant (n = 60)	
Correlating Parameter	Spearman's rho	p value ^b	Spearman's rho	p value	Spearman's rho	p value
Aluminum	0.58	<0.001	0.48	0.042	0.50	<0.001
Calcium	0.59	<0.001	0.70	<0.001	0.46	<0.001
Chlorophyll a	0.73	<0.001	0.78	<0.001	0.81	<0.001
Dissolved organic carbon	0.05	0.758	-0.31	0.063	-0.03	0.840
Dissolved oxygen	0.34	0.046	0.62	<0.001	0.10	0.460
Iron	0.75	<0.001	0.81	<0.001	0.58	<0.001
Magnesium	0.10	0.558	0.02	0.930	0.14	0.277
Potassium	0.11	0.510	0.12	0.474	0.28	0.032
Sodium	-0.21	0.221	0.13	0.447	0.24	0.066
Surface water pH	-0.10	0.570	0.11	0.573	-0.03	0.803
Surface water temperature	0.46	0.005	-0.22	0.252	0.30	0.022
Total nitrogen	0.63	<0.001	0.40	0.004	0.57	<0.001
Total suspended solids	0.84	<0.001	0.62	<0.001	0.82	<0.001

a. n - sample size.

b. probability (p) < 0.05 = significant; p < 0.001 = highly significant.

TP showed positive correlations with Al, Ca, Fe, chlorophyll a, TN, and TSS. Except for a significant correlation with Al during the high flow period (probability [p] = 0.0419), correlations were highly significant and consistent for all flow periods. TP also had highly significant positive correlation with surface water temperature during periods of low flow and stagnation. TP had significant and highly significant positive correlations with DO during the low flow and stagnant periods, respectively. TP showed no empirical association with DOC, Mg, and Na during all periods of the flow events. Correlation of TP with K was significant and positive during the stagnant period only. The highly significant positive correlations of TP with Al, Ca, and Fe suggest the importance of these metal cations in binding with P to form organic/inorganic precipitates. The strong positive correlation between TP and TSS could be related to in-situ production of particulates especially during the stagnant period following periods of flow. The highly significant correlation between TP and TN suggests that the transformations of P in the STAs are strongly coupled to that of nitrogen (N). The relationships among TP, chlorophyll a, surface water temperature, and DO are an indication of productivity. As correlation analysis does not imply causality, a more robust statistical analysis such as principal component or factor analysis will be conducted to identify with greater certainty the factor(s) most important in influencing P retention and cycling along the treatment FW.

SUMMARY

Three controlled flow events were conducted in STA-2 FW 3 under different flow scenarios between February and November 2016. The first flow event consisted of a high flow period, followed by a period of stagnation, and then a post-stagnant period. The second event was preceded by a long period of stagnation, followed by a low flow period, and then a stagnant period before the FW transitioned back to a low flow period. The third flow event consisted of a high flow period, followed by a period of stagnation. Based on autosampler TP data, there was a generally distinct TP concentration gradient from inflow to outflow at all flow periods of each of the three flow events. Consistent with the autosampler data, weekly grab TP showed consistent reduction along the treatment FW at all periods of the flow events. A mean TP concentration reduction of 80% was obtained during the first two flow events and a 60% reduction during the third flow event. Incoming water column TP was dominated by PP, followed by DOP and SRP. Reduction in PP accounted for the majority of the reduction in TP concentration along the treatment FW at all periods of the flow events. Compared to DOP, SRP was reduced much earlier in the FW, indicating that this P fraction was consumed much more readily through biological and physico-chemical processes operating along the front half of the treatment FW. This P reduction pattern is typical of a well performing STA. Residual P pool at the back end of the FW was comprised mainly of PP and DOP at all periods of the flow events. Understanding speciation of P in the water column is critical to knowing the sources and fate of the different species in the STAs. This information will be useful in enhancing our understanding of the P treatment performance along the FW and in developing strategies for achieving water quality goals for the STAs.

TP concentrations were elevated during the stagnant period following the period of high P loading (Flow Events 1 and 3) but not after low P loading (Flow Event 2). The observed increase in TP resulted from a large increase in PP, particularly at the stations closer to the inflow region of the FW (Stations C20 and C56). This indicates PP is generated in-situ when the FW is stagnant. DB Environmental, Inc. (DBE; 2017) reported phytoplankton to be the dominant component of surface water particles characterized during the third flow event during similar stagnant conditions. Measures of phytoplankton density such as chlorophyll concentration, cell density, and biovolume were positively correlated with PP concentration (DBE 2017). The release of P during stagnant conditions has important implications for STA operations and performance, especially because FWs remain stagnant between flow events. One potential management option would be to avoid sending high flows to the STAs after a long period of stagnation, when possible. The flow equalization basins (FEBs), which were recently constructed as part of the *Restoration Strategies Regional Water Quality Plan* (SFWMD 2012) are anticipated to assist in this regard.

One specific objective of this study was to explore correlative relationships between TP and other water quality and field parameters. Strong positive correlations were found between P and some key variables. The metal cations Ca, Al, and Fe along with TN, chlorophyll and TSS were among the many variables that showed highly significant positive correlation with TP during the low flow, high flow, and stagnant periods. As alluded to earlier, correlation does not imply a cause-and-effect relationship; therefore, these empirical relationships should be interpreted with caution. Further analyses will be conducted to identify the factor(s) with significant influence on P retention and cycling along the treatment FW. It is likely that the influencing factors change depending on the location along the FW.

Results from these flow events are still preliminary. Further data analyses are underway, and the results will be presented in future reports. Additional flow events are being conducted in this FW at different flow scenarios. It is anticipated that these events and future flow events for the duration of this study will provide critical information that will help explain the factors and processes influencing STA performance and serve as basis to develop or enhance management strategies that will help the STAs achieve lower TP discharge concentrations.

P FLUX MEASUREMENTS

Mike Jerauld², John Juston² and Tom DeBusk²

INTRODUCTION

This field investigation aims to identify and quantify process-level P flux pathways in the STAs. Specifically, the objectives are to (1) measure net P flux rates along the inflow to outflow gradient of selected FWs, (2) isolate the relative contributions of vegetation and diffusive flux to net P flux, and (3) identify soil variables that influence P flux. The processes contributing to surface water TP concentration include interactions between the soil, water, and biota, particularly primary producers. Based on published information on P cycling in wetlands and historical data in the STAs, it has been hypothesized that there is a relationship between soil P and water column TP through direct diffusion, resuspension, and plant uptake and turnover, but the full extent of this relationship has not yet been quantified. Also, the relative contribution of each of these processes along the inflow to outflow gradient in STA FWs is unknown. Although diffusion of P from porewater to surface water has been studied in many wetlands (Fisher and Reddy 2001, Dunne et al. 2010), there is also evidence that sediment P mining and turnover of aquatic macrophytes (e.g. SAV) can contribute substantially to surface water P concentrations (Juston et al. 2013). It also is possible that burrowing macroinvertebrates can contribute to the flux of soil P to the water column through bioturbation; this phenomenon is currently being investigated under a separate task and discussed at the end of this appendix.

Several terms pertaining to P cycling appear throughout this section and are defined as follows:

- *Flux*: movement or exchange of P between two compartments or matrices (e.g. soil and surface water). The term "flux" is directionless and does not imply movement into or out of any particular compartment.
- *Diffusive flux*: movement of dissolved constituents between soil/porewater and the surface water, as driven by unequal concentrations. According to the laws of diffusion, this flux

² DB Environmental, Inc., Rockledge, Florida.

moves dissolved molecules from regions of higher concentrations to regions of lower concentrations, but otherwise implies no particular direction of movement.

- *Flux potential*: the negative of the slope of porewater P concentrations measured across the -4- to +4-centimeter (cm) soil-water interface (based on porewater equilibrator data). Positive flux potential values indicate an upward P gradient between soil porewater and the lower water column, and negative values indicate a downward gradient between soil porewater and the lower water column.
- Net flux: the combined (net) movement of P into or out of the surface water, including all potential interacting compartments or matrices, such as soil, porewater, algae, or macrophytes. Processes contributing to net flux may include diffusive flux, resuspension, and decomposition. The term "net flux" is directionless, but reflects results in the surface water column.

The following discussion is a summary of findings to date in STA-2 FW 3 on flux trends based on porewater data and in situ chamber water column results.

METHODS

Flux chambers were installed in triplicate in vegetated (VEG) and unvegetated (UNV) patches at inflow (INF), mid-flow (MID), and outflow (OUT) regions of STA-2 FW 3 (total 18 chambers per FW). (Figure 10). Flux measurements were taken using porewater equilibrators (peepers) and in situ flux chambers (5-foot diameter bottomless high-density polypropylene cylinders) (Figures 11 and 12). The chambers have large open windows that allow free water exchange with the surrounding marsh, so that the enclosure experiences the same effects of P loading and other forcing factors as the rest of the FW (Figure 12). Following controlled, prescribed flow events, panels were installed over the windows, isolating an area of the marsh. The water column in the chambers was sampled serially over a 14-day incubation period. Simultaneously, peepers were installed in duplicate outside each set of chambers, and were sampled after 14 days. The change in concentration over time inside the chambers is a measurement of the net flux into or out of the water column from all sources (soil, floc, macrophytes, periphyton, etc.). The static vertical profile of porewater concentrations determined during the peeper installations provided a measure of any net vertical diffusive flux from the soil compartment alone.

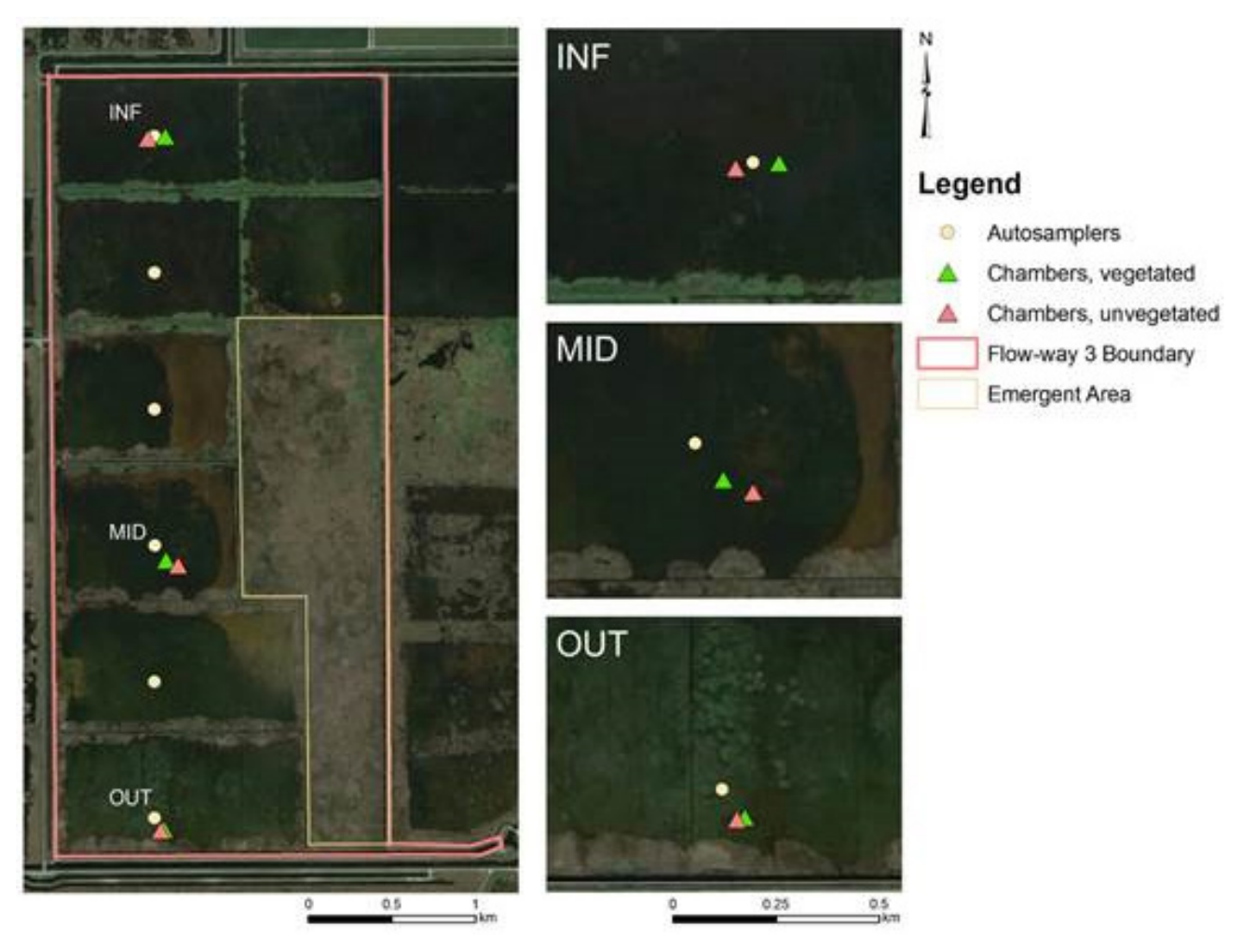


Figure 10. Location of the flux chambers installed in the vegetated (VEG) and unvegetated (UNV) patches of the inflow (INF), midflow (MID), and outflow (OUT) regions of STA-2 FW 3.



Figure 11. Flux chambers installed in the outflow region of STA-2 FW 3, during a chamber closure/monitoring event.

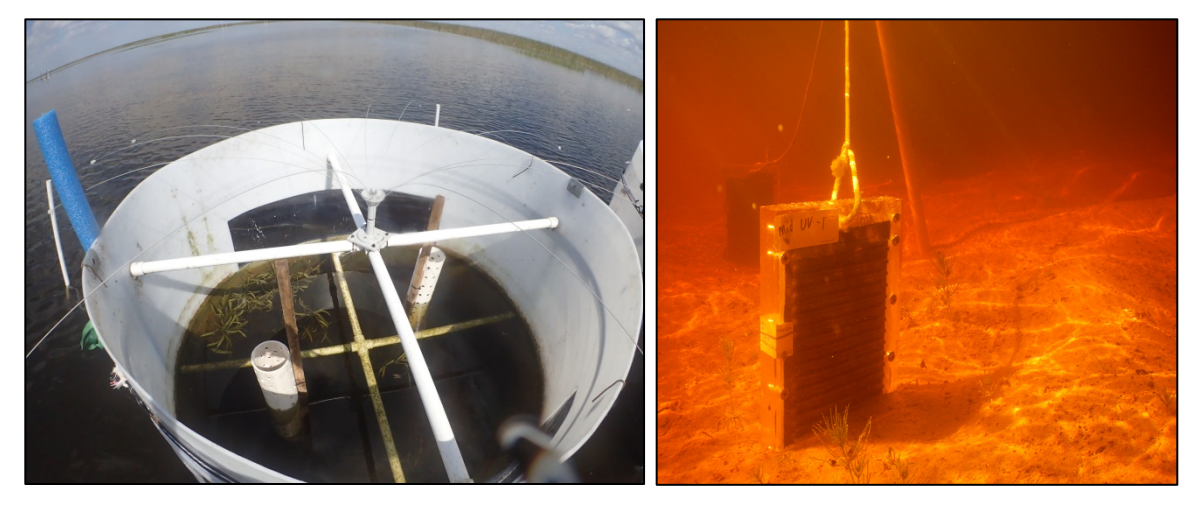


Figure 12. Flux chamber installed in vegetated patch in (left) and porewater equilibrator ("peeper") installed in unvegetated patch in STA-2 FW 3 (right).

The results presented here are from the three events conducted in FW 3 during 2016; two following "high flow" periods (March and November 2016) and one following a no and low flow period (July 2016; **Figure 13**). Complete descriptions of the methodology, event conditions, and full results are available in annual reports (DBE 2016, 2017). The soil samples and peeper data from a 2010 study and peeper results from a 2015 deployment during site selection for chamber installation were also included for additional context and comparison.

RESULTS

This section provides a summary of results from three complete flux monitoring events in STA-2 FW 3 along with data from several prior and complementary peeper and soils studies designed to address the following key study questions:

- What have been the spatial and temporal trends in measured net and diffusive fluxes to date?
- Is there evidence of any relationship between measured chamber responses and estimated flux rates with antecedent P loading rates to STA-2 FW 3?
- Is there evidence of any relationship between measured chamber responses and estimated flux rates with soil P characteristics?

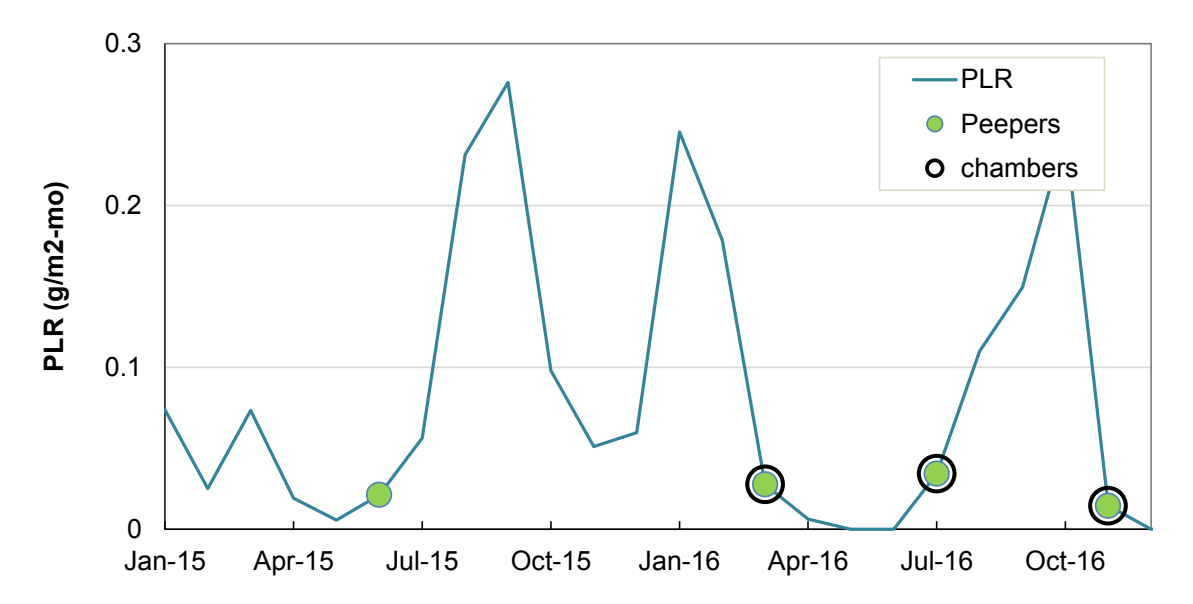


Figure 13. Monthly average phosphorus loading rate (PLR) in grams per square meter per month (g/m2-mo) to STA-2 FW 3. Peeper deployment events are shown with green markers, and chamber closure/monitoring events are shown with open circles.

Antecedent P Loading

One hypothesis has been that measured P flux magnitudes (diffusive and net) might be a function of the antecedent P load recently delivered to the wetland. This is, in part, the reason that the overall P Flux project study design includes flow events at a range of flow/P loading rates. A precise antecedent period during which loading may influence later flux rates is unlikely. Therefore, cumulative prior P loads for 30-, 60-, and 90-day periods were considered for five flux measurement events (**Table 3**), including the three chamber events described above and two prior diffusive flux measurements made in STA-2 FW 3 during 2010 and 2015.

Table 3. Cumulative inflow P loads in grams per square meter (g/m²) prior to four flux-related data collection dates in STA-2 FW 3 by DBE. To date, the three completed chamber events have captured a wide range of antecedent P load conditions.

Sample Date	Description	Antecedent Loading (g/m²)			
Sample Date	Description	30 days	60 days	90 days	
January 2010	DBE sulfur study	0.10	0.10	0.10	
July 2015	Advance peeper deployment	0.02	0.03	0.05	
March 2016	Chamber event – "high flow"	0.17	0.50	0.55	
July/August 2016	Chamber event – "low flow"	0.02	0.04	0.04	
November 2016	Chamber event – "high flow"	0.26	0.43	0.55	

Soil P Conditions

As identified in the original project description and scope of work (DBE 2015), soil P concentrations (especially TP), were thought to be a key driver of internal flux rates. Therefore, soil at the chamber sites were sampled twice in STA-2 FW 3, in correspondence to the first and second chamber closure events (Figure 13), and analyzed for TP and 0.5 molar sodium bicarbonate (NaHCO₃)-extractable P (Olsen P). Soil TP concentrations (0–4 cm from the benthic floc surface) were comparable between the first and second sampling events (Figure 14), but Olsen P, considered here as a measurement surrogate for labile P, showed a stronger trend with distance than TP and a subtle but perhaps important trend with antecedent load (Figure 14). Olsen P levels were lower at all INF and MID collection sites following the three-month stagnant period (July 2016) than following the high flows and loading in the first event (March 2016) (compare Figure 14 and Table 3). Previous analysis of historical STA data (DBE 2016) showed a strong positive relationship between labile soil P (Olsen P, in particular, but other soil P tests provided similar results) and diffusive flux potential. Based on these combined findings, there is evidence that Olsen P is a more sensitive indicator of recent P load effects than soil TP.

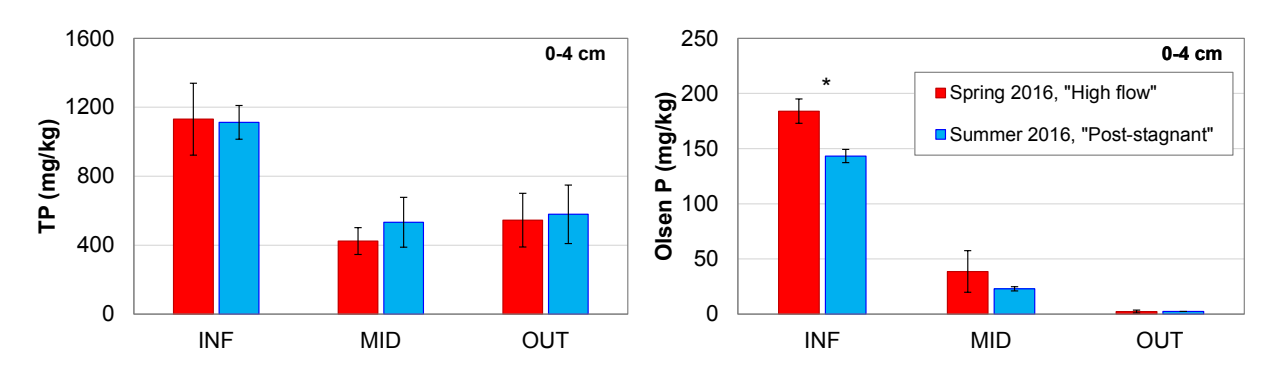


Figure 14. Average (sample size [n] = 4) soil TP and 0.5M NaHCO₃-extractable (Olsen) P concentrations in milligrams per kilogram (mg/kg) in the top 0–4 cm soils in study patches at the INF, MID, and OUT regions in STA-2 FW 3 in March 2016 following a period of high flow/load and in July/August 2016 following a period of no inflow/load. Error bars give the range of observed concentrations. Event means were significantly different (p < 0.05 based on a two-way t-test).

Synthesis of Porewater and Diffusion Results

Vertical water P concentration gradients were calculated from peeper data across the porewater-surface water interface, specifically from 4 cm below the floc surface (porewater) to 4 cm above the floc surface (water column). This gradient provides an indication of the vertical potential for Fickian diffusive fluxes; further assumptions on floc density and path tortuosity allowed for estimates of actual flux rates. The potential for diffusion from porewater to surface water was consistently elevated but also variable between events at the INF region. Comparatively, the potential for diffusive fluxes was non-detectable at the outflow region (OUT; **Figure 15**). These results suggest that vertical diffusive fluxes, i.e. from soil porewater to the water column, are insignificant in the back-end marsh, the region just upstream of the discharge structure. This can be attributed to the low accretion of TP in soil in this region of the treatment FW, since most of the P load has been retained in the inflow region of the FW.

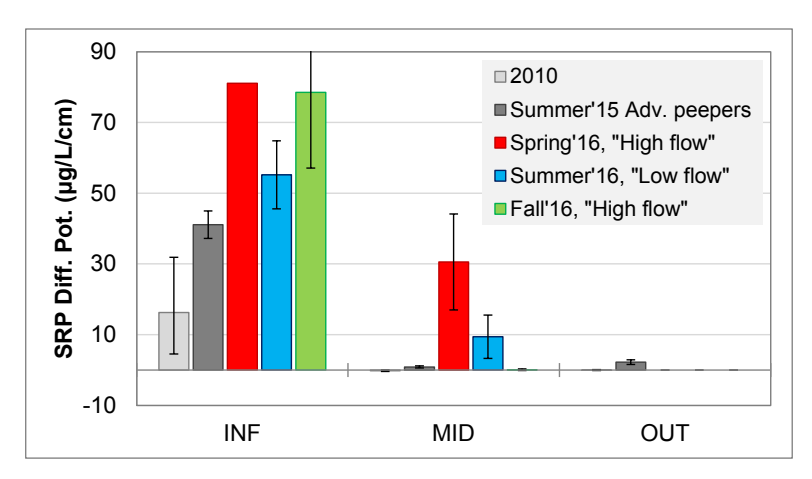


Figure 15. Mean (n = 1–4) SRP diffusion potential (Diff. Pot.) in micrograms per liter per centimeter (μ g/L/cm) across the sediment-water interface (+4 to -4 cm) at inflow (C20), mid (C128), and outflow (C200) regions in STA-2 FW 3 on five measurement dates. Positive values indicate a vertical concentration gradient from porewater to the lower water column. Error bars represent the range of observed values.

The March and July/August 2016 measurements of porewater SRP gradients associated with chamber closure events could be assessed against soil P data measured at the time of the closure events (**Figure 16**). Diffusion potentials (calculated from SRP concentration gradients) correlated strongly (between events) with soil Olsen P (**Figure 16b**), but less so to soil TP (**Figure 16a**). This confirms similar results from previous analysis of historical STA data (DBE 2016). Although the highest diffusion potentials have been measured at INF following the two high loading events, in general, no clear relationship is observed between the diffusion potential and the magnitude of the antecedent load (**Figure 17**). These relationships will continue to be monitored as additional measurement events are conducted.

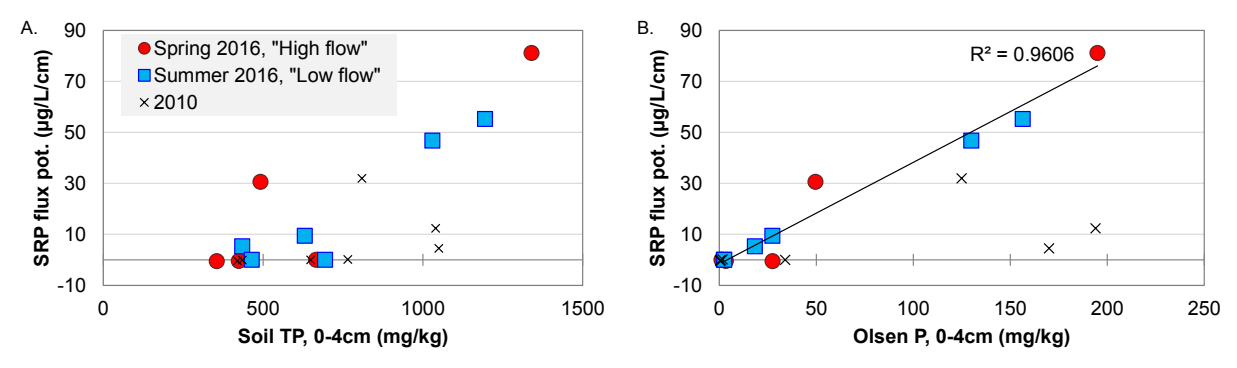


Figure 16. Mean (n = 2) SRP diffusive flux potentials (pot.) in micrograms per liter per centimeter $(\mu g/L/cm)$ with respect to (A) soil TP and (B) soil Olsen P in STA-2 FW 3.

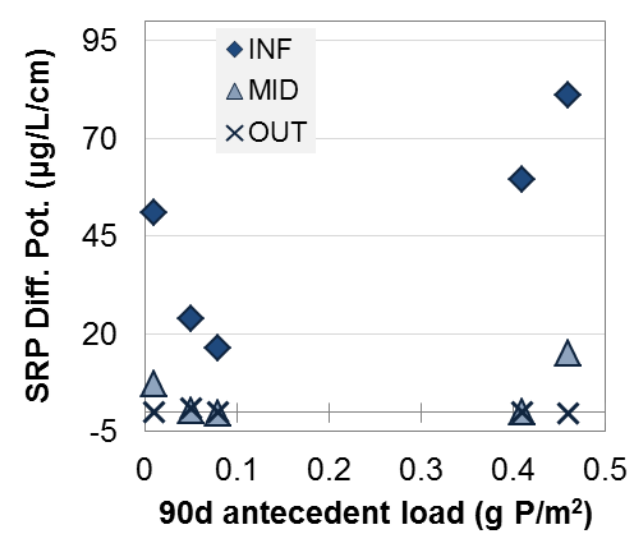


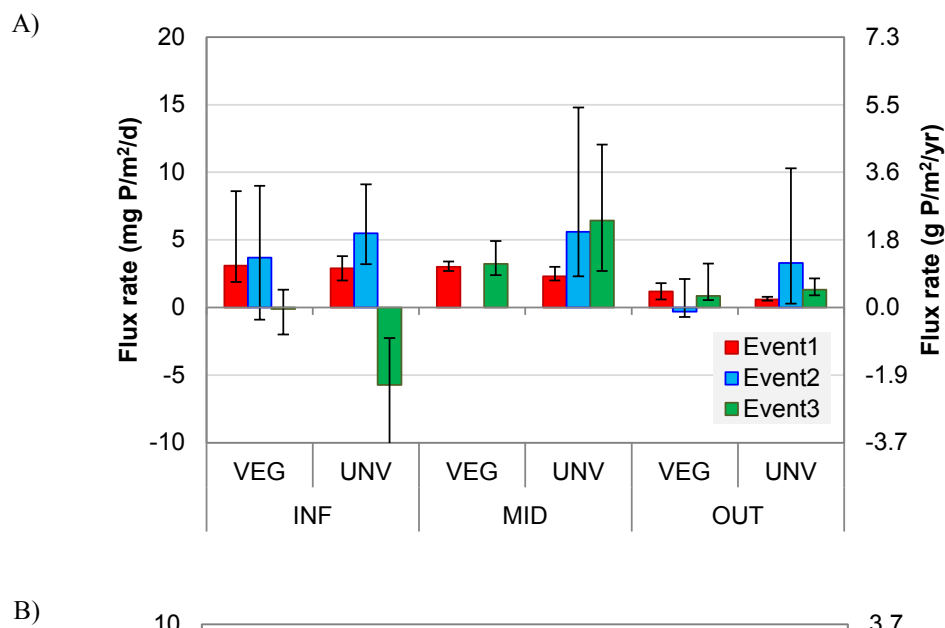
Figure 17. Relationship between mean (n = 2–4) SRP diffusive flux potential (Diff. Pot.) in micrograms per liter per centimeter (μ g/L/cm) in STA-2 FW 3 and the cumulative areal P load in the 90 days preceding each flux measurement.

Chamber Responses and Net TP Fluxes

Net TP flux rates were estimated from chamber time series responses using a provisional curve-fitting approach to help assess the net change in P over time ($\Delta P/\Delta t$) over the 14-day closure period. The process of complementing the curve-fitting analysis approach with a process-based interpretation using the K-C Model (Kadlec and Wallace 2009) in batch mode is ongoing. As the study proceeds, focus will be more on rigorous comparisons of marsh responses inside and outside the flux chambers, during the marsh-wide no flow intervals that accompany closure events.

From the curve-fitting results, provisional net flux rates obtained from individual measurement events ranged from -5.5 mg P/m²/d (i.e. net uptake; Event 3 at INF UNV) to about 6.5 mg P/m²/d (Event 3 at MID UNV), with most of this variability occurring within UNV chambers at INF and MID. At OUT, net flux rates varied within a narrower range, -0.3 to 1.3 mg P/m²/d (**Figure 18a**). Average flux magnitudes at each site across the three measurements to date ranged from about 0.5 mg P/m²/d (OUT VEG) to about 5 mg P/m²/d (MID UNV) (or 0.2–1.8 g P/m²/yr on an annual basis), and have been somewhat higher in UNV chambers than VEG chambers at MID and OUT (**Figure 18b**). Field observations suggesting phytoplankton

develops more abundantly in the UNV chambers are supported by P speciation data showing that the increase in TP is principally as PP (Figure 19).



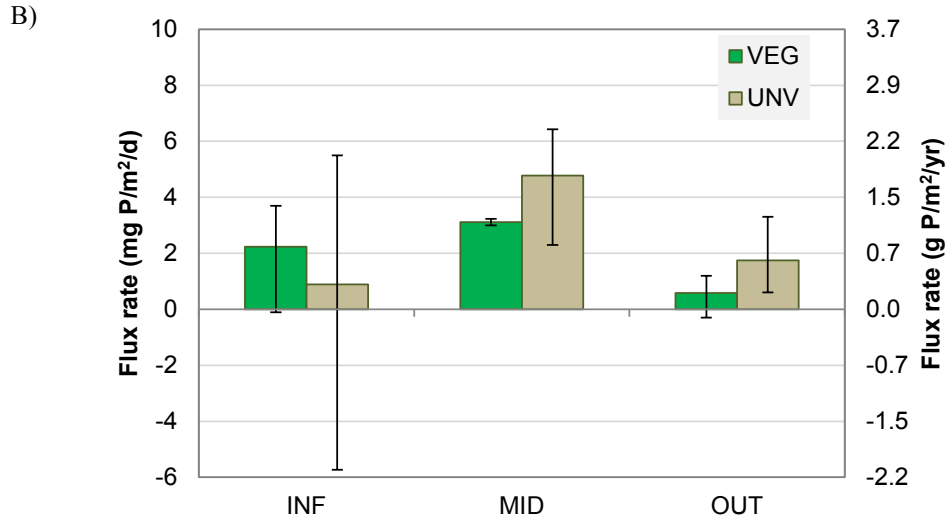


Figure 18. Estimates of net TP flux rates to the water column in triplicate sealed in situ chambers in VEG and UNV patches at INF (C20), MID (C128) and OUT (C200) regions of STA-2 FW 3. These values represent the rate of concentration change until the waters reached 90% of the equlibrium concentration, as determined by fitting a sigmoid curve to the time series of TP concentrations inside the chambers. The top panel shows the rates for each individual chamber event; error bars give the 5–95% confidence interval. The bottom panel shows each chamber group averaged across events; error bars give the range of individual event means. The magnitudes of these reported flux rates are provisional, and may change in future reports as we continue to refine calculation methods.

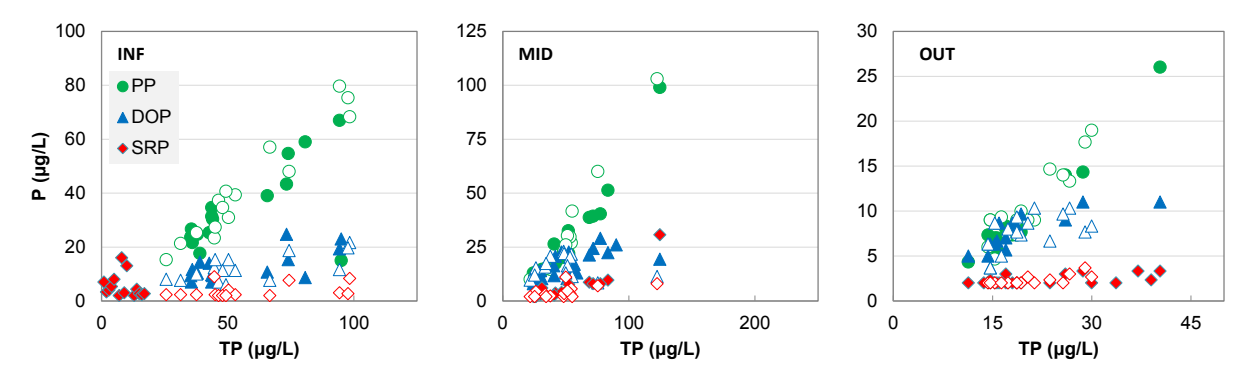


Figure 19. Cross-plots of concentrations of P species (PP, DOP, and SRP) relative to TP concentrations in sealed chambers at INF (C20), MID (C128) and OUT (C200) locations in STA-2 FW 3 during the three 2016 flux chamber closure/measurement events. Each point represents the average of triplicate chambers on each measurement date (n = 5 per closure event). Filled points represent VEG chambers; open points represent UNV chambers.

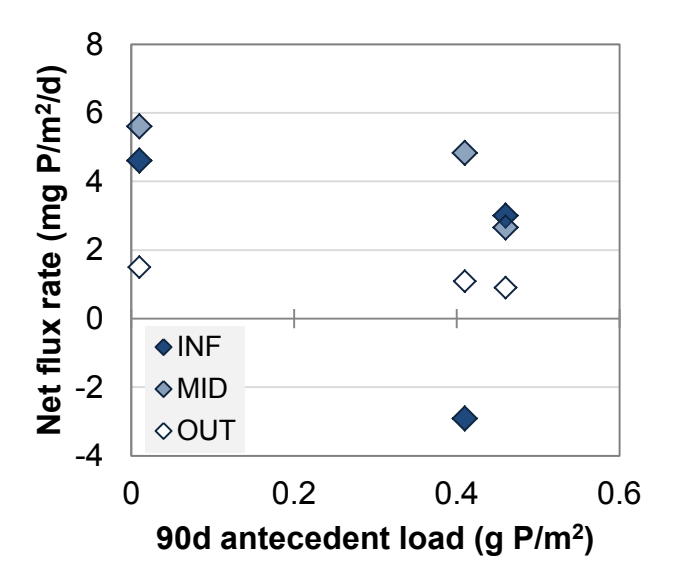


Figure 20. Average (n = 6) net TP flux rates to the water column in sealed in situ chambers with respect to the cumulative P load to STA-2 FW 3 in the 90-day period preceding the flux measurement event. Since all chambers at a site receive the same antecedent load, flux rates are averaged across vegetation treatment within sites. (Note: $g P/m^2 - grams P per square meter.)$

To date, there is also no evidence of a longitudinal spatial pattern in the provisional net flux rates from the chamber closures, although values at OUT tended to be slightly lower (**Figure 18**). This is in contrast to the strong longitudinal patterns observed in soil diffusive fluxes (**Figure 15**). To date, there is also no discernible temporal trend in net flux rates (**Figure 18a**).

Net flux rates were not significantly related to the immediate (90-day) antecedent P loading rate (**Figure 20**), although the sample size (n = 3) was still low for a definitive assessment. Also, net flux rates were not correlated with either soil TP or Olsen P measurements (**Figure 21**), although such an assessment may have been influenced by the relatively high flux rates at the MID site, despite the low-P soil conditions there. Net flux rates across the three measurement events were not well correlated to the peeper-estimated diffusion potentials (**Figure 22**).

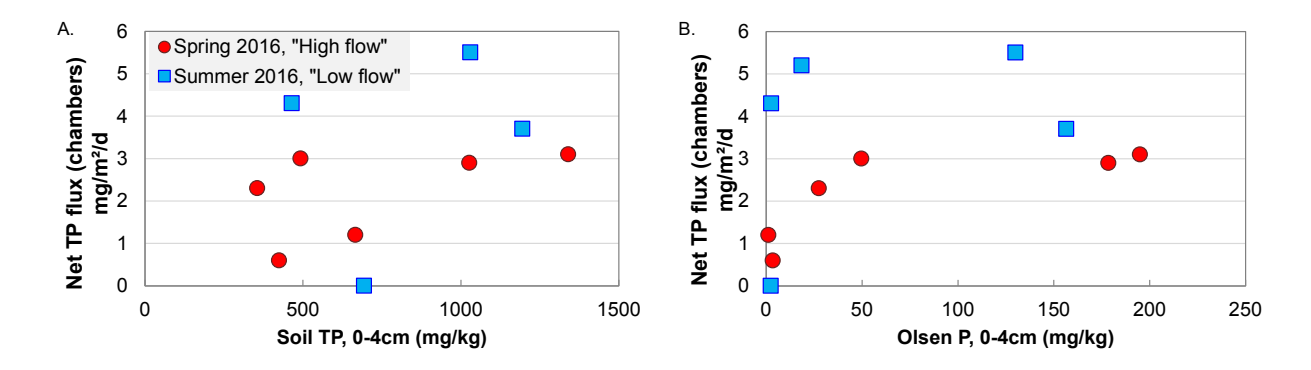


Figure 21. Net TP flux rates to the water column in sealed in situ chambers with respect to soil (A) TP and (B) Olsen P in STA-2 FW 3. (Note: mg/kg – milligrams per kilogram and mg/m²/d – milligrams per square meter per day.)

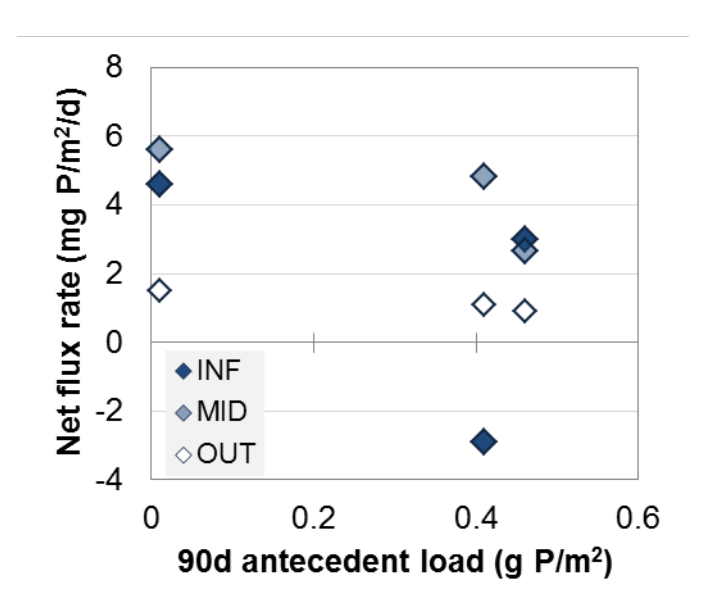


Figure 22. Average (n = 3) net TP flux rates to the water column in sealed in situ chambers with respect to peeper-estimated P diffusion potentials. (Note: $g P/m^2 - grams P$ per square meter.)

In summary, there are no strong temporal or spatial patterns, or relationships with antecedent load or soil P conditions, from the combined chamber experiments to date (n = 3). However, net fluxes have also consistently far exceeded estimated diffusive fluxes. One possible interpretation is that these apparent net internal P loads are occurring at a steady rate along the treatment gradient, as suggested by the preliminary findings (**Figure 16a**), possibly originated from or through various biotic sources. However, additional future chamber events and possibly other measurements will help evaluate this and other potential mechanisms.

SUMMARY

Five measurements of diffusive flux potential using peepers have been made in STA-2 FW 3 since 2010. Results from these events indicate that vertical diffusive fluxes likely produce an internal load to water column P in the INF and MID regions of STA-2 FW 3 that also varies in magnitude over time. In contrast, there has consistently been no evidence of vertical diffusion in the outflow region of the FW. Data

indicates a correlation between these clear longitudinal gradients in vertical diffusion potential and gradients in labile soil P concentrations, which, at least at the inflow region, may in turn be affected by short-term antecedent P loading. On the other hand, estimates of net internal loads measured from the in situ batch process chamber responses are much higher than the measured diffusive fluxes (at all three positions along the gradient) and show no strong temporal or spatial patterns, or relationships with shortterm antecedent load or soil P conditions. This interpretation of chamber response data is provisional, and subject to further analysis of these data and results of future measurement events. However, combined, these results suggest that there are likely substantial contributions to net internal fluxes from other soil and/or biotic processes aside from Fickian diffusion from soil porewater. This hypothesis is supported by poor relationships observed between measured net flux rates and soil/porewater variables, such as soil P concentration and diffusion rate. Accumulating P in chamber time series responses tended to occur as PP; characterization of this PP is under way. Finally, all monitoring events have found positive net flux rates in the outflow region, where diffusion potentials were negligible, so as noted above, these as-yet unidentified flux mechanisms seem to be providing an important, possibly even dominant, control on STA outflow concentrations. Efforts toward identifying additional sources and mechanisms of P release are under way. Continued flux measurements during different flow conditions in STA-2 FW 3 and in other FWs should help provide further insights.

SPATIAL PATTERNS OF P CONCENTRATIONS AND STORAGES IN THE STAS

Rupesh K. Bhomia¹, Todd Osborne¹, Odi Villapando, and K. Ramesh Reddy¹

INTRODUCTION

Sustainable removal of macroelements such as P, carbon (C), N, and sulfur (S) by wetlands depends upon production and burial of refractory residuals created by microbial, periphyton, and vegetation communities. P management in the Everglades STAs has been a major focus of SFWMD staff and ongoing monitoring of P concentrations in inflow and outflow water provides indication of P retention by these STAs. Soils and sediments store most of the P relative to other ecosystem components (plant biomass and plant litter) via processes that include surface adsorption on minerals, precipitation, immobilization, and accretion of matter, which consists of organic matter and other relatively recalcitrant constituents. The main objective of this study is to obtain an accurate estimate of nutrient storages in floc and soils while documenting soil conditions in the STAs. The spatial patterns in concentration and storage of macroelements including P, C, N, and S were evaluated to determine the influence of long-term nutrient loading and vegetation types: EAV and SAV. Other macroelements such as K, Ca, Mg, Fe, and Al were also determined in soil samples, but only soil P concentrations and storages are presented in this section. At a later stage, this study will yield process-level information on P uptake and release, and transport of P across the soil-water interface, as well as movement of P within the soil profile.

METHODS

The STA FWs chosen for this study either have EAV or SAV. The four FWs included FW 1 (EAV) and FW 3 (SAV) of STA-2, and Cells 3A (EAV) and 3B (SAV) of STA-3/4. These test sites were selected as a representative example of FWs that have achieved outflow TP concentration between 13 and 30 μ g/L, and offer an opportunity to study different FW configurations, vegetation communities, and soil conditions. Soil sampling locations were selected from the existing grid established by District scientists or contractors

for the purposes of soil and vegetation monitoring and survey (Figure 23). The grid soil sampling pattern chosen for this work ensures equal representation of all areas within the test FWs.

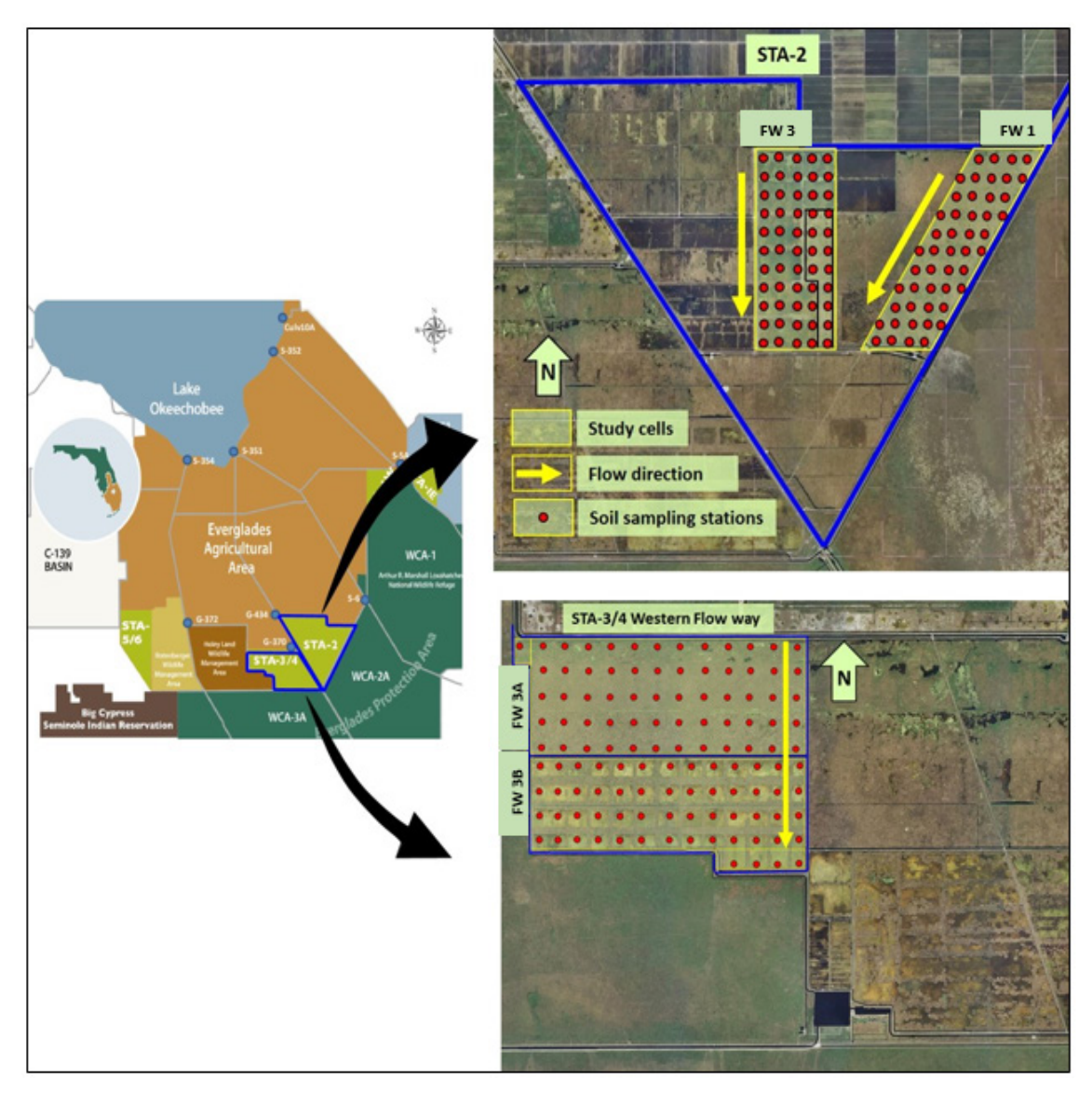


Figure 23. Soil sampling locations in STA-2 FWs 1 and 3 and STA-3/4 Cells 3A and 3B.

Intact soil cores were collected using 10-cm diameter polycarbonate core tubes. Soil cores were stored in a cold room (~4 degrees Celsius [° C]) before separating into plant litter (when present), floc, recently accreted soil, and pre-STA soil (original soil) fractions. Floc depth was measured by allowing flocculent (unconsolidated) material to settle in a plastic core tube for 3 to 4 hours and after settling floc was poured into a plastic bag. Underlying recently accreted soil and pre-STA soil layers were differentiated based on texture and color of the material, and section thickness was recorded. The thickness (depth) of the underlying pre-STA soil varied from one location to another depending on the total length of the soil core taken. Sample pH and bulk-density was determined in the lab, and samples were homogenized after drying. Macroelemental content was determined in these homogenized samples at the District's Chemistry Lab. The geostatistical wizard extension of ArcGIS Version 10.4 (ESRI, Redlands, CA) was used to create

kriging models and dot maps (for trend validation) of all macroelements in litter, floc, recently accreted soil, and pre-STA soil.

RESULTS

Spatial Patterns of P in STA-2

A total of 55 soil cores from STA-2 FW 1 (representing EAV FWs) and 61 soil cores from STA-2 FW 3 were obtained for spatial soil characterization (**Table 4**). Twelve of the 61 soil cores obtained from FW 3, were in *Typha* dominated region and therefore classified as EAV, while the remaining 49 cores were representative of an SAV-dominated region.

Study Location	Intact Cores	Litter	Floc	Recently Accreted Soil	Pre-STA
STA-2 FW 1	55	47	55	55	55
STA-2 FW 3	61	6	61	60	60
STA-3/4 Cell 3A	65	58	65	65	65
STA-3/4 Cell 3B	60	2	60	60	60

Table 4. Number of intact soil cores and core section samples collected for spatial soil characterization.

Spatial trends in litter TP for FW 3, while very limited in scope (only EAV portion of sites had appreciable litter), suggested enrichment of litter along the flow path (**Figure 24**). This spatial trend was much more evident in FW 1 as indicated by distinct spatial gradients in litter TP. Floc TP exhibited similar trends of high enrichment proximal to inflows with concentrations diminishing towards the south (outflows). Enrichment of floc in FW 1 was substantially higher and more spatially extensive compared to FW 3. Trends in floc TP in FW 3 suggest a dominant FW has been established on the east side of the FW or this signature could be a result of EAV vegetation presence on the southeastern side of the FW.

Trends in TP concentrations of recently accreted soil were similar to those of floc in that FW 1 exhibited a clear linear decline in TP from inflows to the outflows and the overall level of enrichment was higher in FW 1 than in FW 3 (**Figure 25**). Approximately 50% of the front half of FW 1 had recently accreted soil TP content > 750 milligrams per kilogram (mg/kg). Likewise, spatial trends in EAV region of FW 3 (southeastern side) had higher TP concentration than adjacent SAV regions. TP concentrations decreased with depth: floc > recently accreted soil > pre-STA soils. P enrichment of pre-STA soils was minimal. Pre-STA soils in FW 1 exhibited some enrichment along the FW boundaries, which is more evident in the dot maps than the geostatistical model (**Figure 25**). FW 3 was generally higher in pre-STA soil TP concentration across most sites with a noted cluster of enrichment in the northern third of the FW. No clear spatial trends of TP concentration were observed in FW 1 pre-STA soils. However, TP concentration of pre-STA soils of FW 1 (EAV) were lower than those measured in FW 3 (SAV), suggesting some mining of subsurface P by *Typha* spp. (**Figure 25**).

Geospatial model trends suggest TP gradients from inflows to outflows in floc, litter, recently accreted soil, and pre-STA soils. An interesting exception appears to be the pre-STA soils in STA-2 FW 1, which showed increased soil TP along the border canals. Patterns of TP in all depth increments can be indicative of flow pathways with enriched areas having the greatest exposure to P laden waters. For example, recently accreted soil in STA-2 FW 3 has soil TP values > 750 mg/kg extending farther south on the east side of the FW than the west side, suggesting either preferential flow on the east side and thus greater P enrichment or this could be a result of EAV vegetation along the southeastern side of FW 3.

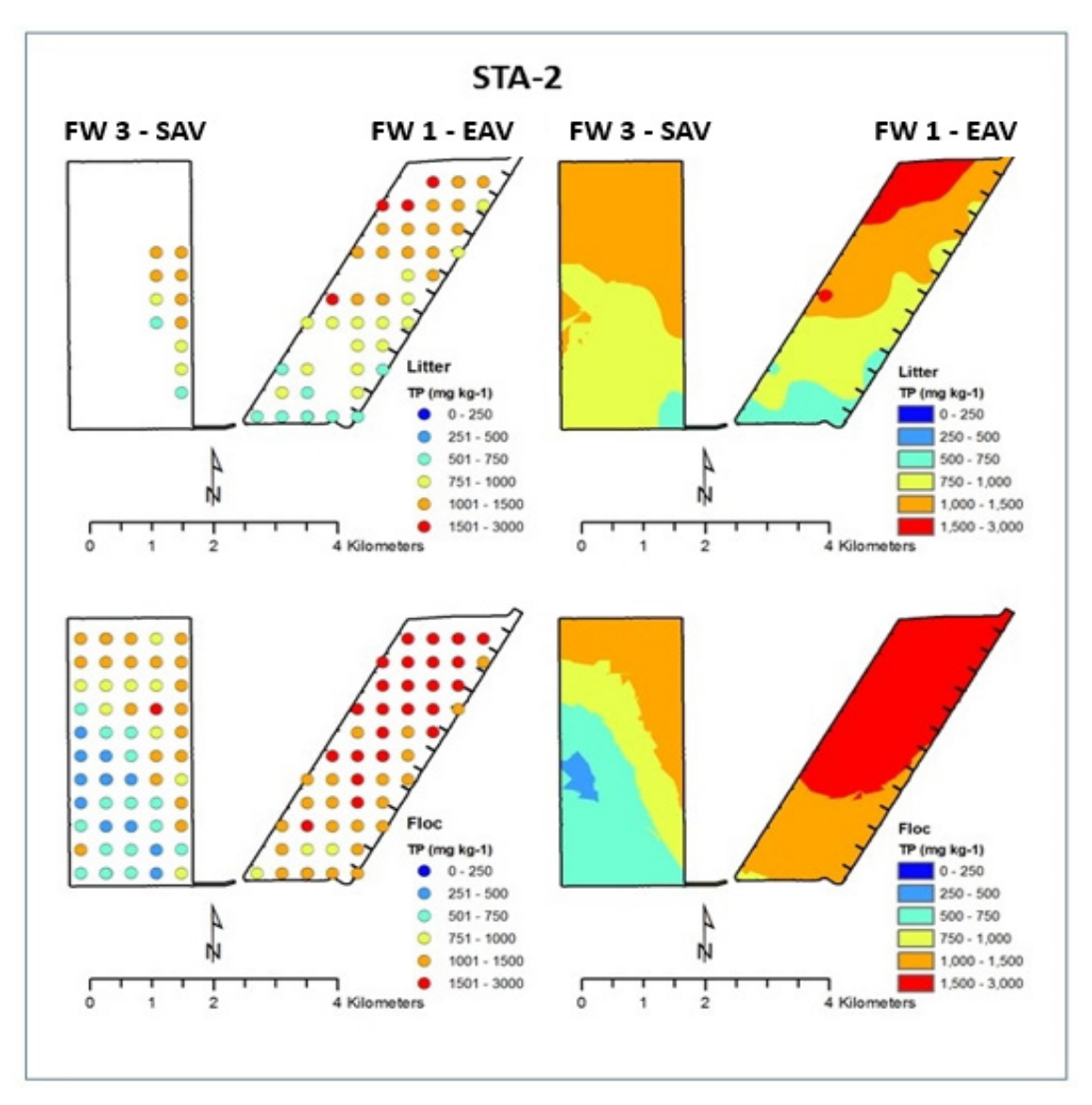


Figure 24. Spatial distribution of TP concentrations (mg/kg) in litter and floc sections of the intact soil cores collected from STA-2 FW 1 (EAV) and FW 3 (SAV).

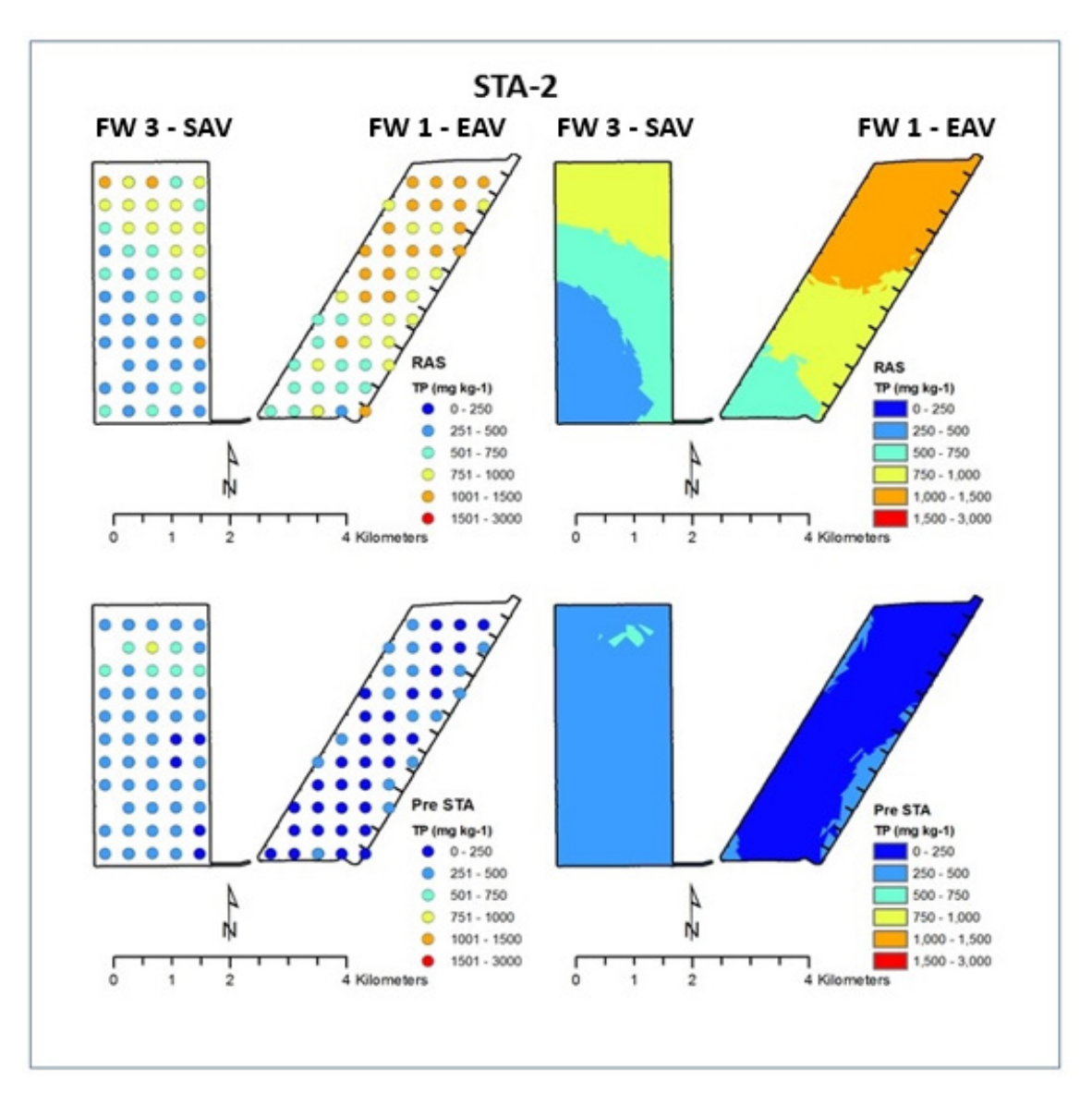


Figure 25. Spatial distribution of TP concentrations (mg/kg) in recently accreted soil (RAS) and pre-STA soil sections of the intact soil cores collected from STA-2 FW 1 (EAV) and FW 3 (SAV).

P storage in recently accreted soil suggests declining trends with distance from inflow in both FWs (**Table 5**). Perhaps more importantly, P storages in FW 1 are relatively low in comparison to FW 3, indicating the relative roles of EAV and SAV in floc production and thus P storage in this portion of the soil profile. Phosphorus storage in the floc and recently accreted soil represents P accretion since the operation of STA-2 began while P storage in pre-STA soils represents P present in soils prior to the operation of STA-2. Although the P enrichment in pre-STA soils is lower than floc and recently accreted soil, high bulk density and deeper soil depths resulted in high P storage. Since pre-STA sections were thicker (~17 cm) than floc (~8 cm) and recently accreted soil (~3 cm) sections (**Table 5**), overall P storage per unit area in this layer was greater than the other two layers.

Ρ Ca Vegetation Sample Depth **Bulk Density** P Mass Count рΗ **Concentration Concentration** Type Type (cm) (g/cc) (g/m²) (g/kg) (mg/kg) **STA-2 FW 1** EAV N/A b 31 ± 2.1 N/A Litter 47 N/A N/A $1,079 \pm 73$ **EAV** Floc 55 7.7 ± 0.4 7.3 ± 0 0.02 ± 0.00 68 ± 5.4 $1,626 \pm 61$ 2.0 ± 0.1 Recently EAV 2.5 ± 0.2 7.7 ± 0 0.08 ± 0.00 Accreted 55 75. ± 7.4 944 ± 31 1.7 ± 0.2 Soil **EAV** Pre-STA 55 19.1 ± 0.3 7.1 ± 0 0.13 ± 0.00 40 ± 0.5 236 ± 8 6.1 ± 0.3 **STA-2 FW 3 EAV** Litter 11 N/A N/A N/A 87 ± 14.8 $1,041 \pm 61$ N/A **EAV** Floc 12 10.0 ± 2.1 7.6 ± 0.1 0.04 ± 0.00 141 ± 21.8 $1,145 \pm 85$ 4.5 ± 1.1 Recently **EAV** 3.5 ± 0.9 7.9 ± 0.1 0.13 ± 0.01 156 ± 25.9 645 ± 58 Accreted 12 2.4 ± 0.4 Soil **EAV** Pre-STA 18.4 ± 1.1 7.4 ± 0.1 0.15 ± 0.01 272 ± 12 7.2 ± 0.6 12 48 ± 1.6 SAV Floc 10.7 ± 0.5 7.5 ± 0 0.11 ± 0.00 295 ± 6 701 ± 40 10.7 ± 0.5 49 Recently SAV Accreted 48 3.0 ± 0.2 8.0 ± 0 0.19 ± 0.01 219 ± 9.8 605 ± 33 3.0 ± 0.2 Soil SAV Pre-STA 48 16.4 ± 0.7 7.3 ± 0 0.23 ± 0.01 47 ± 3.1 437 ± 29

Table 5. Selected properties of core section samples from STA-2 FWs 1 and 3. Values are arithmetic averages \pm standard error of the mean. ^a

Spatial Patterns of P in STA-3/4

In STA-3/4, Cells 3A (EAV) and 3B (SAV) were selected for soil characterization. Unlike STA-2, where each FW operates individually, the treatment train in STA-3/4 included both Cell 3A (EAV) and Cell 3B (SAV) with Cell 3A receiving the inflow water first and Cell 3B receiving Cell 3A effluent flows. These two cells have been in operation since 2006. Sixty-five (65) soil cores from STA-3/4 Cell 3A and 56 soil cores from Cell 3B were obtained for spatial soil characterization (**Table 4**).

Spatial trends in litter TP for Cell 3A (EAV), suggested P enrichment of litter with a decreasing trend from the inflow to outflow, however, this trend is not very clear as there are no observable patterns visible in the dot maps (**Figure 26**). Kriging models show a more evident trend; however, this is to be viewed with caution as Cell 3B only had two points where appreciable litter was found and thus these points are highly leveraged in the model of Cell 3B. Floc TP exhibited trends of highest enrichment proximal to inflows in Cell 3A with concentrations diminishing towards the south (outflows) in Cell 3B. Because these two cells have different vegetation, EAV in 3A and SAV in 3B, spatial patterns of enrichment of floc in Cell 3A is substantially higher than in Cell 3B (**Figure 26**). Since Cell 3B receives outflow water from Cell 3A, overall P loading in this cell is lower than in Cell 3A, which may result in lower floc TP concentration in Cell 3B. Trends in floc TP in the southern portion of Cell 3A and the northern portion of Cell 3B suggest an established breakpoint in floc concentration at the change point in vegetation.

a. Key to units: cm – centimeter; g/cc – grams per cubic centimeter; g/kg – grams per kilogram; g/m² – grams per square meter; and mg/kg – milligram per kilogram.

b. N/A - not applicable.

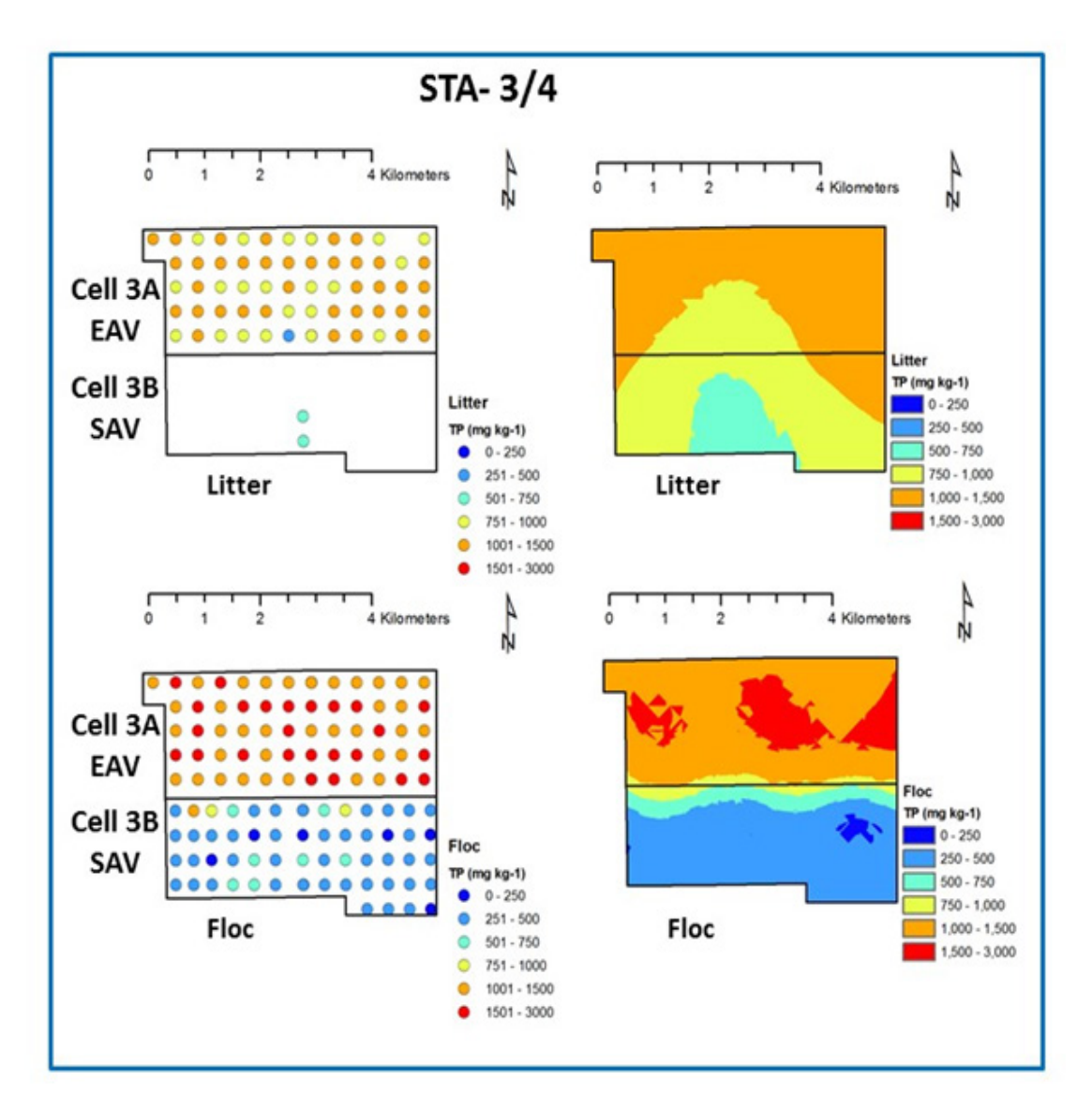


Figure 26. Spatial distribution of TP concentrations (mg/kg) in litter and floc sections of intact soil cores collected from STA-3/4 Cells 3A and 3B.

Trends in recently accreted soil TP were similar to those of floc in that Cells 3A and 3B exhibited steady declines in TP from inflow to the outflow and the overall level of enrichment was higher in Cell 3A than in Cell 3B (**Figure 27**). Likewise, spatial trends suggest a breakpoint at the levee between Cell 3A and Cell 3B, which also demarcates the change in vegetation from EAV to SAV dominance. It is also noteworthy that while TP trends in floc and recently accreted soil were similar, the recently accreted soil was lower in P concentration than the floc component directly above it in the profile. Pre-STA soils were found to be much more homogenous with spatial trends suggesting enrichment of this soil's profile with P from inflows. Both dot maps and the general spatial model support this assertion. Overall, TP spatial trends suggest strong gradients from inflows to outflows in litter, floc, recently accreted soil, and pre-STA soils and a strong breakpoint at the confluence of Cell 3A and Cell 3B.

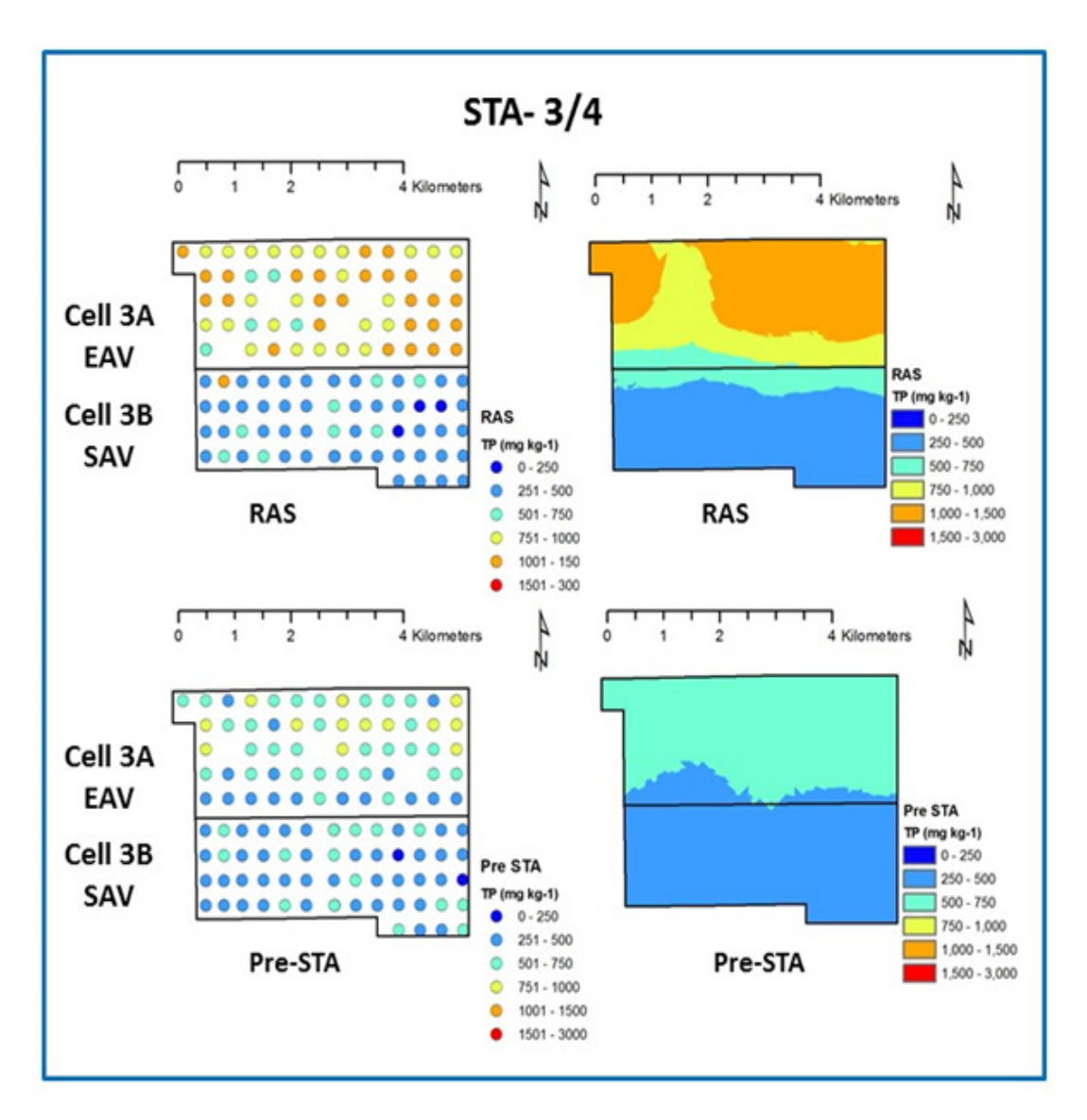


Figure 27. Spatial distribution of TP concentrations (mg/kg) in recently accreted soil (RAS) and pre-STA soil sections of intact soil cores collected from STA-3/4 Cells 3A and 3B.

P storage in recently accreted soil declined with distance from the inflow in both cells (**Figures 26** and **27**). Because these cells operate in series, with outflow from Cell 3A serving as inflow into Cell 3B, P storage was higher in Cell 3A than in Cell 3B. The trends in TP concentration in EAV and SAV cells of STA-3/4 were consistent with trends observed in STA-2. However, P storages in floc and RAS layers of STA-2 FW 3 (SAV) were much higher than those found in STA-3/4 Cell 3B (SAV). Storage patterns in pre-STA soils for both FWs were higher than both floc and recently accreted soil in all cases perhaps because pre-STA section was thicker than floc and recently accreted soil layers (**Table 6**).

Table 6. Selected properties of soil core section samples from STA-3/4 Cell 3A and Cell 3B. Values are arithmetic averages \pm standard error of the mean. ^a

Vegetation Type	Sample Type	Count	Depth	рН	Bulk Density (g/cc)	Ca Concentration (g/Kg)	P Concentration (mg/Kg)	P Mass (g/m²)
STA-3/4 Cell 3A								
EAV	Litter	63	N/A ^b	N/A	N/A	37 ± 2.4	1,044 ± 20	N/A
EAV	Floc	65	8.0 ± 0.7	7.3 ± 0	0.03 ± 0.00	70 ± 5.5	1,443 ± 24	3.4 ± 0.5
EAV	Recently Accreted Soil	60	2.8 ± 0.2	7.6 ± 0	0.10 ± 0.01	97 ± 7.1	1,053 ± 28	3.0± 0.4
EAV	Pre-STA	65	14.3 ± 0.6	7.3 ± 0	0.30 ± 0.01	58 ± 2.4	624 ± 31	28.1 ± 2.0
STA-3/4 Cell 3B								
SAV	Litter	2	N/A	N/A	N/A	163 ± 21.9	625 ± 106	N/A
SAV	Floc	60	9.1 ± 0.4	7.6 ± 0	0.11 ± 0.00	316 ± 4.2	395 ± 24	3.7 ± 0.2
SAV	Recently Accreted Soil	60	2.3 ± 0.1	8.1 ± 0	0.13 ± 0.01	277 ± 4.7	399 ± 19	1.2 ± 0.1
SAV	Pre-STA	60	16.3 ± 0.5	7.4 ± 0	0.22 ± 0.01	50 ± 1.9	448 ± 12	15.9 ± 0.6

a. Key to units: cm – centimeter; g/cc – grams per cubic centimeter; g/kg – grams per kilogram; g/m² – grams per square meter; and mg/kg – milligram per kilogram.

PRELIMINARY CONCLUSIONS

The two STAs provide an interesting contrast to study differences in P uptake and storage mechanisms due to FW configuration and how different vegetation (EAV versus SAV) influences P removal from the water column. In STA-2, FW 1 (EAV) and FW 3 (SAV) operate in parallel, where both FWs receive similar inflow P concentration and P mass loading, however STA-3/4 Cell 3A (EAV) and Cell 3B (SAV) operate in series where inflow P concentration and P mass loading to Cell 3B is much less than Cell 3A. This difference is evident in the longitudinal profiles of P concentration in floc and recently accreted soil of studied FWs. Phosphorus concentrations in floc and RAS at the front end of studied FWs were much higher (>1,000 mg/kg) than floc and soil P concentrations observed at the enriched areas of WCAs of the Everglades basin (Childers 2003, DeBusk 2001). Overall STA soils appear to be accumulating much greater quantities of P in comparison to P delivered and stored in WCAs soils. Since floc and recently accreted soil are representative of material that has accrued after the STAs became operational, the differences in the nutrient signatures in EAV and SAV sites are indicative of the characteristics of nutrient uptake and biogeochemical processing occurring in these FWs. In STA-2, both FW 1 and FW 3 show a distinct pattern of enrichment proximal to the inflow region, but in STA-3/4, the enriched zone is limited to the front end of Cell 3A. Removal of P from influent water is primarily achieved through biotic and abiotic processes including uptake by vegetation followed by growth, senescence, and sequestration as detritus into accreting soils, and precipitation reactions in soil and water column. In EAV FWs, vegetation uptake and storage is known to be the predominant P removal pathway, while precipitation of P with Ca (and other mineral cations) is more prevalent in SAV FWs. In SAV FWs, low plant biomass and rapid turnover rates also result in short-term P storage in vegetative tissue.

A distinct signature in floc and recently accreted soil fractions was observed in EAV and SAV FWs, whereas pre-STA soil characteristics were similar in both EAV and SAV sites. Pre-STA soils were uniform, however, in STA-2 FW 3, a noted cluster of enrichment in the northern third of the FW was observed. TP concentrations of pre-STA soils of FW 1 (EAV) were lower than those measured in FW 3 (SAV),

b. N/A = not applicable.

suggesting that some mining of subsurface P by cattails is taking place. Typically, SAV floc and recently accreted soil had higher bulk density than in the EAV FWs. Concentrations of P were lower in all soil sections in the SAV system STA-2 FW 3, but Ca concentrations were higher (**Table 5**). This probably is the reason for higher bulk density in floc and soil sections. Thus, the mass storages of macronutrients and Ca, which is a function of bulk density, were higher in SAV sites in comparison to EAV sites.

In STA-3/4, TP concentrations associated with the floc, recently accreted soil, and pre-STA soil were generally higher for Cell 3A than Cell 3B. This is evidenced by a distinct breakpoint in TP concentrations where vegetation transitions from EAV to SAV. For both cells, there was a more pronounced longitudinal gradient in floc TP concentrations than in recently accreted soil and pre-STA soil. TP concentrations in the pre-STA soil lacked spatial variability but were higher in Cell 3A than in Cell 3B. Because these cells operate in series, with the outflow from Cell 3A serving as inflow into Cell 3B, the observed differences in concentration between cells and among components (i.e. floc, recently accreted soil, and pre-STA) can be attributed to historic P loadings into this FW. P storages were generally higher in Cell 3A in comparison to Cell 3B. This was in contrast to STA-2 FW 3, where SAV FWs had higher P storages. FW configuration and different P loadings may have accounted for this difference. While TP concentrations were lower in all soil sections of Cell 3B, Ca concentrations were higher compared to Cell 3A (Table 6). This might have affected the bulk density of Cell 3B floc and soil sections, but the effect was not as noteworthy as observed in STA-2 FW 3. The mass storages of macronutrients and Ca were higher in the floc layer of SAV Cell 3B, but for the recently accreted soil and pre-STA soil layer, P and Ca storages were higher in EAV Cell 3A. In the EAV system, P transformations are primarily driven by biotic reactions and the forms of P and storage are tightly coupled to organic matter accumulation in the soil and water column. In the SAV system, P transformations are driven by abiotic and biotic reactions and the forms of P and storage are influenced by the physico-chemical environment altered by SAV. These apparent differences in P processing within wetlands dominated by different vegetation types could dictate environmental stability of sequestered P in the STAs. The reactivity of various P pools in accreted soils eventually would determine the long-term sustainability of STAs, as these systems continue to operate and remove P from the surface runoff.

EFFECTS OF FAUNAL COMMUNITIES ON THE WATER QUALITY IN THE EVERGLADES STA

Nathan Evans³, Joel Trexler³, and Mark Cook

INTRODUCTION

The influence of animals on P forms, fluxes, and transformations in the Everglades STAs has been identified as a potential constraint to their efficient management for P removal. Fauna, including waterbirds, fish, and macroinvertebrates, are increasingly recognized as important in nutrient cycling in aquatic ecosystems (Vanni 2002, Doughty et al. 2016). The abundance and mix of aquatic animals can affect water column nutrient concentration through several pathways. First, animals function as a source of internal nutrient loading by directly mobilizing benthic or particulate nutrients through their feeding and excretion (Vanni et al. 2006). Second, they can have important indirect effects through modifications of the environment (e.g. bioturbation; Vanni et al. 2006) and by top-down consumptive effects involving predator limitation of food resources and cascading interactive effects (Dorn 2013, Kellog and Dorn 2012). Bioturbation elevates water column nutrients through the resuspension of benthic nutrients and seston. Topdown effects may impact nutrient cycles if they alter the abundance of key grazers or bioturbators, altering

³ Florida International University, Miami, FL

the efficiency of animal-mediated nutrient cycles. Finally, aquatic animals can act as important P sinks and vectors of P-transport (Vanni et al. 2006), especially by large, mobile animals such as birds, crocodilians, and fish.

While the ecological literature points to a pivotal role of fauna in STA nutrient cycling, the direct and indirect roles of animals on nutrient cycles have not been studied or estimated in the STAs, and their impacts on P transformations are currently unknown. To gain an improved understanding of the magnitudes of these processes within the STAs and ultimately the effect of fauna on water column total P concentrations in the STA outflow FWs, this study will (1) estimate abundance of waterbirds (STAs 1E, 1W) and (2), estimate standing stock biomass and community compositional data of large bodied fishes (STA-1 East [STA-1E], STA-1 West [STA-1W], and STA-2), and small bodied fish and aquatic macroinvertebrates (STA-2), (3) estimate mass-specific P consumption and excretion rates of the most abundant species, and (4) experimentally evaluate the potential of benthic aquatic species to enhance water column nutrient concentrations through bioturbation. Biomass and excretion estimates will be combined to estimate areal (per ha) P excretion by the entire faunal assemblage in STA-2 (i.e. rates of P released to the water column via excretion, micrograms P per hectare per hour [µg P/ha/h]). Excreted loads of P will be compared to external loads of P and the nutrient demand of SAV through collaboration with vegetation scientists. Bioturbation estimates will be used to evaluate the potential of animals to alter the efficiency of benthic sequestration of total P that may be included in future P budgets and provide guidance to management actions aimed at improving P retention efficiency. This section summarizes the initial data from this study.

METHODS

Waterbird Surveys

Wintering populations of waterbirds of the orders Cicconiformes (storks), Pelicaniformes (herons, ibises, and spoonbills), Gruiformes (rails and limpkin) and Anseriformes (ducks), were quantified using aerial video surveys. Surveys were conducted of the outflow FWs in three STAs (STA-1E, STA-1W, and STA-2) (**Figure 28**) on a biweekly basis from October through May between 2014 and 2016.

Aerial video surveys typically involve a special case of plot sampling, called strip-transect sampling (e.g. Briggs et al. 1985), in which the camera covers long, narrow strips vertically below the aircraft. Strip-transect sampling assumes that the sampled plots constitute a random sample that is representative of the entire study region, and that all individuals within a strip are detected. Thus, the number of birds counted divided by the total plot area gives an estimate of the avian density of the plot. The mean density for the plots is estimated and then applied to the entire study region.

The survey design comprised a systematic grid of parallel strip-transects oriented perpendicular to the long axis of the wetland FWs (east to west) with a minimum separation distance of 500 meters (m) between successive transects. This maximized the number of transects within each STA (minimum of 20 transects per STA) to improve precision, while minimizing the likelihood that any birds disturbed during the survey were double-counted in subsequent transects. Locations of transects were determined using the survey design tool in the software Distance 6.1 (Thomas et al. 2010), which randomly placed a grid of transect lines over the outflow (SAV) FWs of a given STA. The strip transects covered approximately 10% of the total area of the outflow FWs of each STA.

Aerial surveys were conducted using a Bell 407 helicopter. A GoPro Hero3+ camera was attached to the pitot tube on the nose cone of the helicopter facing forward and downward at 45 degrees from the vertical. Transects were flown at a speed of 60 knots and at an altitude of 30 m, which produced a video footprint 65 m in width. Flights started between 7:30 a.m. and 800 a.m., and the three STA transects were completed in a single 3-hour flight. Flights were conducted when wind speeds were less than 30 kilometers per hour, there was no rain or fog, and visibility was > 10 kilometers.

The video data is currently being analyzed by two trained reviewers. Double reviews are being conducted on 20% of the data, which was selected at random. Density estimates for each species will be analyzed using a uniform detection function in Distance (Thomas et al. 2010).

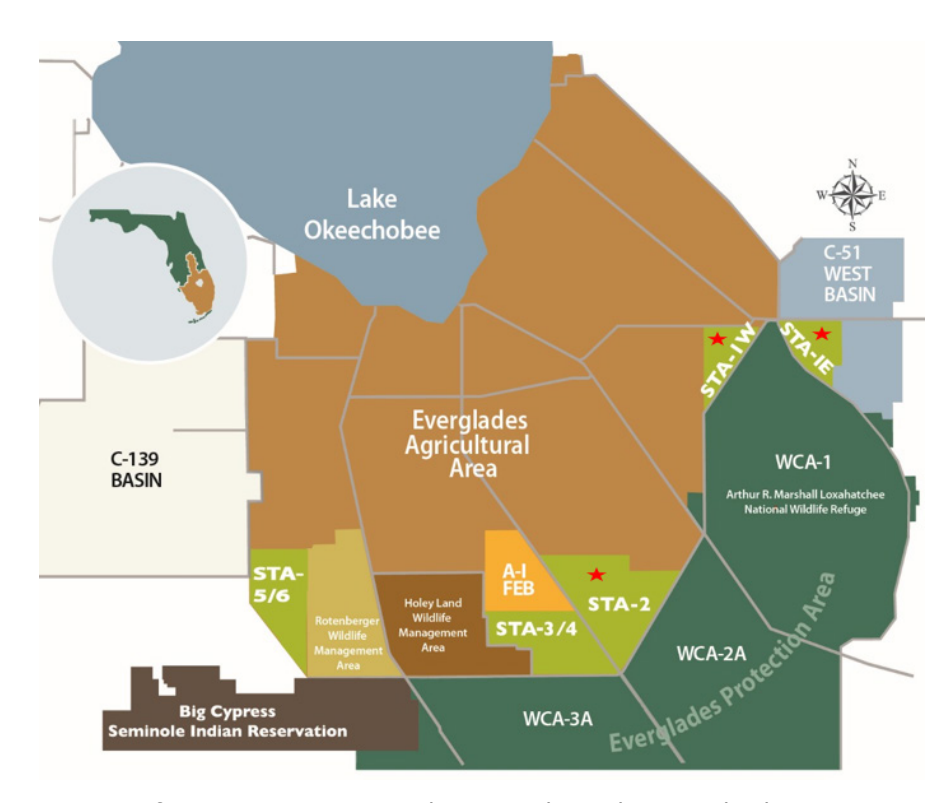


Figure 28. Location of STA-1E, STA-1W, and STA-2 where the waterbird surveys were conducted.

Quantifying Aquatic Faunal Biomass and Community Composition

Fish and macroinvertebrate surveys of biomass and community composition of STA-2 outflow FWs 3, 4, 5, and 6, Shark River Slough (SRS), WCA-3, and Taylor Slough (TSL) were conducted in 2016. STA-2 samples were collected from June 16 to July 6, 2016 (sample size [n] = 124 throws) while WCA-3 samples were collected from July 11 to July 28, 2016 (n = 150 throws). TSL and SRS samples (n = 175 and n = 126 throws, respectively) were collected from July 5 to July 20, 2016. Large fish (≥ 8 cm standard length [SL]) abundance was quantified as average catch-per-unit-effort (CPUE) based on replicated 5-minute electrofishing transects (Chick et al. 1999). Small fish (≤ 8 cm SL) and macroinvertebrates were quantified using 1-square meter (m^2) throw traps (Dorn et al. 2005, Jordan et al. 1997) in open water and SAV habitats to estimate density and species composition. All captured individuals were euthanized with MS222, preserved with formalin in the field, and processed in the lab in the weeks following the sampling.

To incorporate spatial variation in animal biomass and associated habitat types within the STA outflow FWs, a random sampling design stratified by vegetation type was used. Sampling effort (124 throw trap samples and 16 electrofishing transects) was proportionally stratified based on the areal coverage of the four dominant habitats (*Ceratophyllum demersum*, *Najas* spp., *Chara* spp., and open water) found in the SAV outflow FWs. To capture seasonal variation, throw trap samples were collected in June and September 2016. Electrofishing transect samples were collected in STA-2 during February, April, and October 2016. In addition, four electrofishing transect samples per outflow FW were collected in STA-1E (FWs 4S, 4N, and 6) and STA-1W (FWs 1B, 2B, 3, 4, 5B1, and 5B2). An additional set of throw trap and electrofishing samples were collected in March 2017, and are currently being processed.

To evaluate how the STA-2 fish and macroinvertebrate communities compare to other areas of the Everglades, the results of the STA field surveys were compared to the data from surveys conducted in SRS, WCA-3, and TSL including marshes south of the C-111 canal (TSL) during similar months in 2016. Average throw trap fish and macroinvertebrate densities and biomasses were compared among the four Everglades regions via a repeated measures analysis of variation (rmANOVA). Likewise, average electrofishing CPUE for the four regions were compared using rmANOVA. Average fish and macroinvertebrate species richness (number of unique species) of the throw trap samples was evaluated via rarefaction analysis. Rarefaction analysis enables comparison of samples with differing sampling effort and species density. All statistical analyses were performed in R 3.3.1 (R Development Core Team, Vienna).

PRELIMINARY RESULTS

Waterbirds

While insufficient video data have been analyzed to estimate avian population sizes and densities at the scale of the STA outflow FWs, a preliminary examination of the count data suggests that some groups of waterbirds can be extremely abundant and have the potential to significantly impact water quality in the treatment train. A single video survey of STA-1W and STA-2, selected at random shows large counts of American coots (*Fulica americana*) (14,605 and 12,130 individuals, respectively), which overwinter in the STAs and feed largely on SAV (**Figure 29**). The final estimated population sizes will be considerably greater than these counts because the surveys covered only 10% of the area of the open FWs.

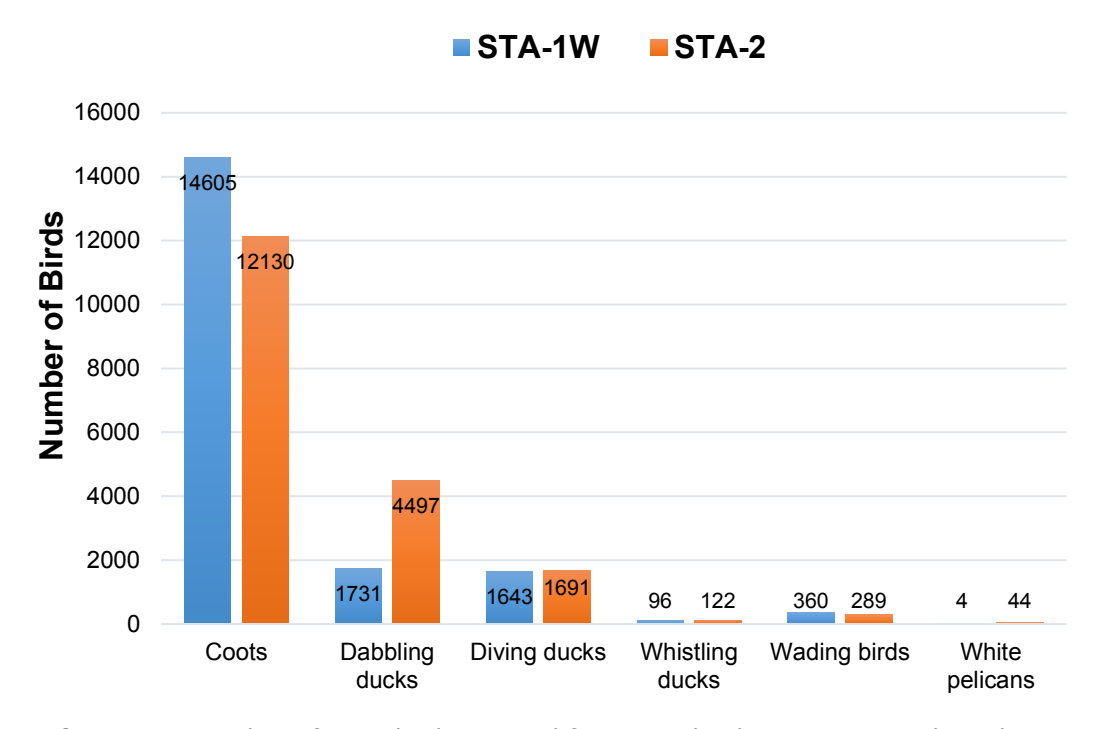


Figure 29. Number of waterbirds counted from aerial video surveys conducted at STA-1W and STA-2 during a single, representative aerial survey in 2016. Note that the final population estimates are expected to be considerably greater than these counts because the surveys covered only 10% of the area of the open FWs.

Assuming that the average coot consumes 90 grams (g) of SAV (dry weight) and excretes 54 g of guano (dry weight) per day (Kear 2005), then the 14,605 birds counted in STA-1W are consuming approximately 1,314 kilograms (kg) SAV and producing 789 kg of guano per day. Given that coot guano comprises 1.4% P (Kear 2005) and the population winters in the STAs for approximately 6 months of the year (182 days), these coots are recycling a total of 2,016 kg of TP per year. At the scale of the entire STA (STA-1W is 26,483,000 m²), this amounts to an areal internal TP loading of 0.08 grams per square meter per year (g/m²/yr). This loading represents 4% of the total external stormwater inputs of 1.9 g/m²/yr for this STA, and is a new contribution to the STA P budget that has not previously been considered. While 4% represents only a modest contribution to total P loading, it may nonetheless have a significant impact on the ability of this STA to meet the WQBEL given the fine margins involved. Moreover, 4% is a highly conservative estimate. The current count used in the calculation is based on a survey of 10% of the area of the open FWs; when this is replaced by the much larger population estimate for the entire open FW area, and the population estimates for other waterbird species are also included, total population estimates for STA-1W open FWs could approach 200,000 birds. If so, then the contribution to loading by waterfowl could very well equal that of the external loading. When interacting effects are also considered (e.g. considerable reductions in SAV cover by waterbird consumption), it seems likely that TP concentrations in the outflow FWs could be increased substantially by the presence of waterbirds.

Small-bodied Fish and Macroinvertebrate Community Composition

In total, 9,654 fishes and 7,302 macroinvertebrates were collected in the combined 248 throw trap samples (1-m² throws) conducted in STA-2 during the June and September 2016 sampling events. Total fish species richness consisted of 21 species and included the clown goby (*Microgobius gulosus*), a species that has not previously been observed in the freshwater Everglades outside of coastal river estuaries (Loftus and Kushlan 1987), but is known to be established in Lake Okeechobee (Ager 1971). Total macroinvertebrate species richness consisted of 33 species. Mean fish density (individuals/m²; \pm standard error [SE]) was 42.5 ± 5.0 in June and 35.5 ± 3.7 in September (**Figure 30**). Mean macroinvertebrate densities were significantly greater than densities observed in the other regions of the Everglades during the same time periods (**Figures 30** and **31**). The high densities of fishes and macroinvertebrates in STA-2 suggest the potential for fishes and macroinvertebrates to have substantial impacts on water column P and N concentrations via both nutrient recycling and nutrient translocation. Despite the higher densities of fishes and macroinvertebrates in STA-2 relative to the other regions of the Everglades, rarefaction analysis of fish (**Figure 32**) and macroinvertebrate (**Figure 33**) species richness suggest the sample abundance-corrected species richness is lower in STA-2 than in the other regions of the Everglades.

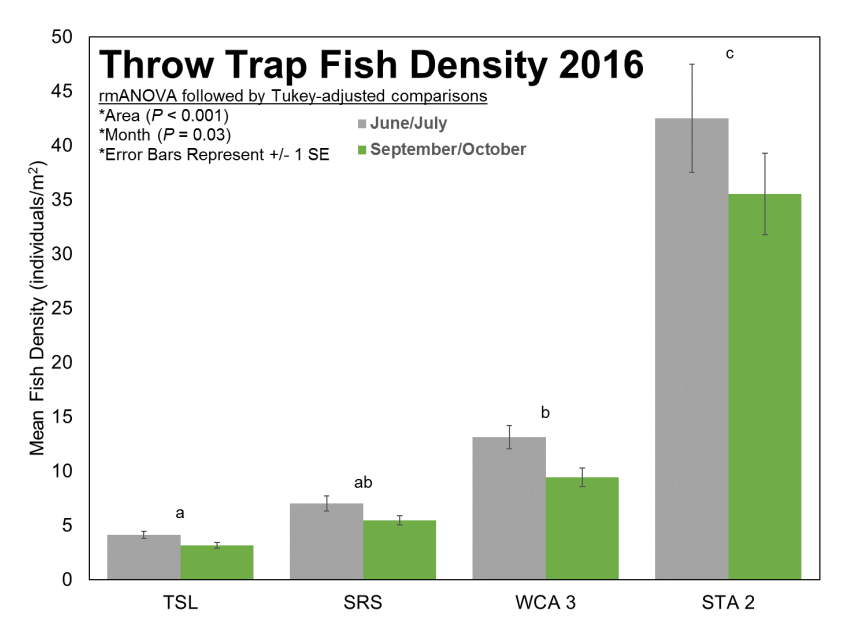


Figure 30. Mean fish density estimated from throw trap samples collected in summer (grey bars) and fall (green bars) 2016. Mean discrimination testing results are indicated by the letters above each column with different letters indicating the mean fish densities between the Everglades areas are significantly different (probability $[p] \le 0.05$).

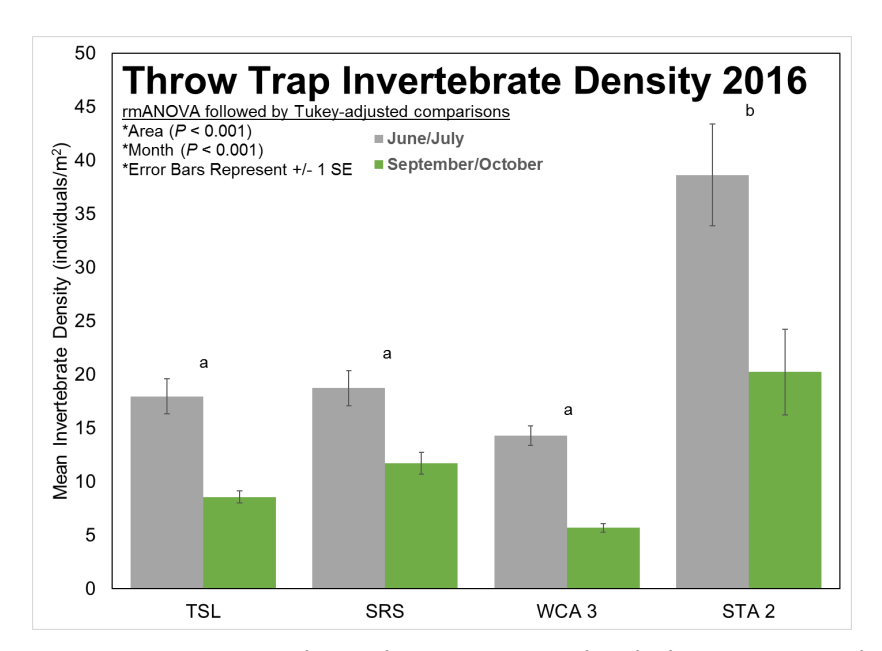


Figure 31. Mean macroinvertebrate density estimated with throw trap samples collected in summer (grey bars) and fall (green bars) 2016. Mean discrimination testing results are indicated by the letters above each column with different letters indicating the mean macroinvertebrate densities between the Everglades areas are significantly different ($p \le 0.05$).

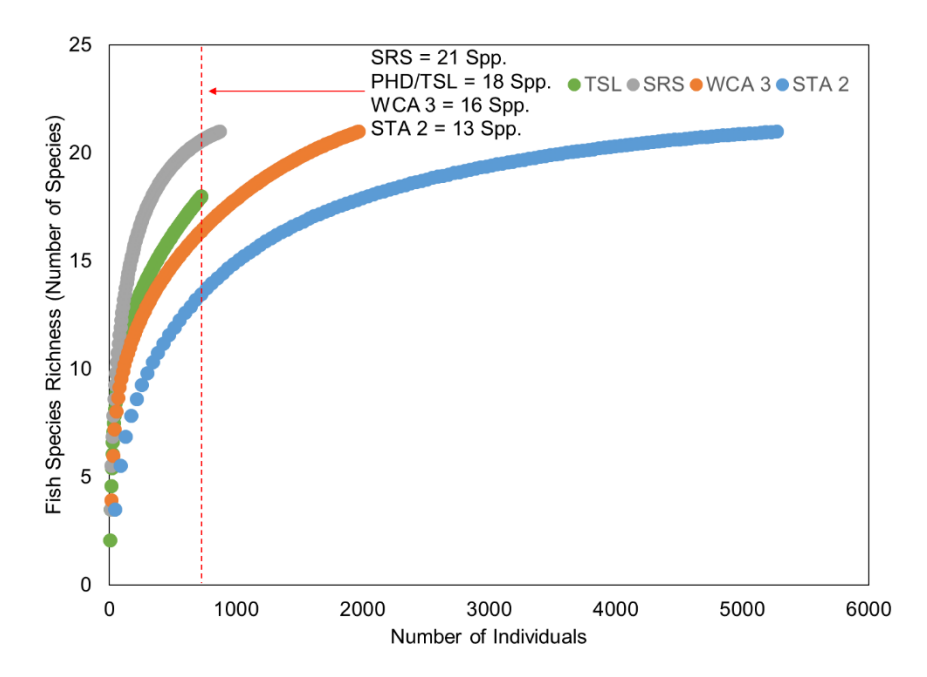


Figure 32. Fish species richness rarefaction curves based on the June-July throw trap samples collected in STA-2 (n = 124 throws), SRS (n = 126 throws), WCA-3 (n = 150 throws), and TSL (n = 175 throws) in 2016. The dashed red line indicates the cumulative maximum number of individuals collected in the region with the lowest mean number of individuals per sample (TSL) and represents the maximum point at which species richness can be compared among the four regions. (Note: PHD – southeast Taylor Slough/C-111 panhandle basin.)

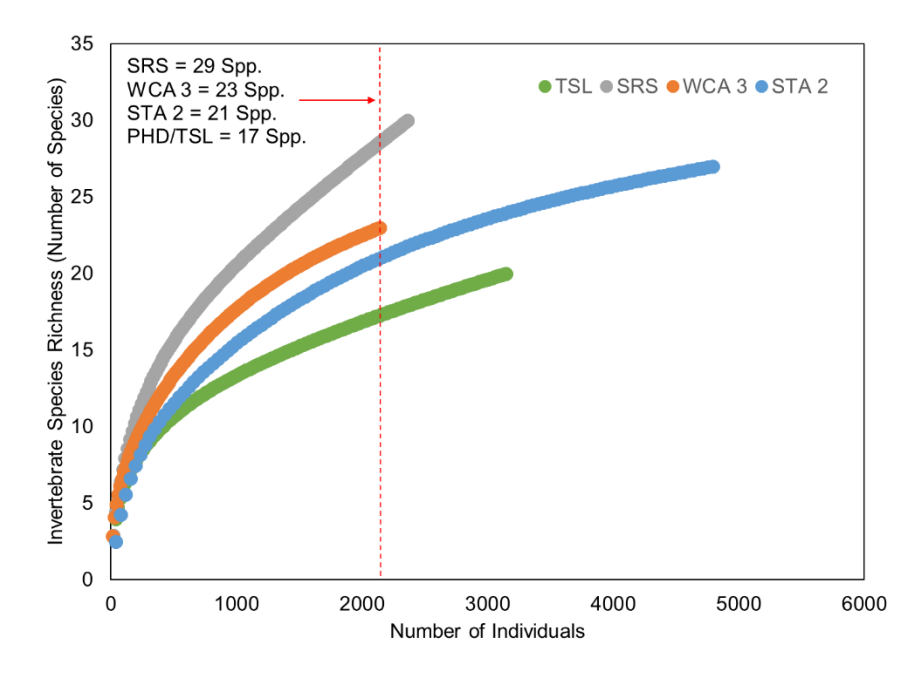


Figure 33. Macroinvertebrate species richness rarefaction curves based on the June-July throw trap samples collected in STA-2 (n=124 throws), SRS (n=126 throws), WCA-3 (n=150 throws), and TSL (n=175 throws) in 2016. The dashed red line indicates the cumulative maximum number of individuals collected in the region with the lowest mean number of individuals per sample (WCA-3) and represents the maximum point at which species richness can be compared among the four regions.

Large-bodied Fish Assemblage Composition

A total of 1,645 individuals were collected during 175 electrofishing transects conducted in STA-2, STA-1E, and STA-1W during 2016 (Table 7). Total species richness across all sampling events was 20 species in STA-2, 20 species in STA-1E, and 19 species in STA-1W. Catch structure was relatively consistent among the sampling events with largemouth bass (Micropterus salmoides), sunfish (Lepomis spp.), Seminole killifish (Fundulus seminolis), and blue tilapia (Oreochromis aureus) among the most commonly collected species (Table 7). Mean CPUE in April was greater than in February and October (rmANOVA, probability [p] < 0.001). These differences in catches appears to be heavily influenced by the disproportionally greater catches in STA-1W during the April sampling (Figure 34) and relatively small catches in STA-2 and STA-1W during the October sampling. Mean CPUE did not differ among SRS, WCA-3, or TSL (see mean separation notation, Figure 34); mean CPUE in STA-1W and STA-1E were greater than in these non-STA regions. Mean CPUE in STA-2 was greater than in SRS and WCA-3 but not TSL. However, the high CPUE in the TSL area is largely because of the non-native Asian swamp eel (Monopterus albus), which invaded this region in 2012 and has reached high densities. Therefore, the CPUE in the STAs suggests that abundances of large-bodied fishes are greater there than in other regions of the Everglades. These results also suggest the potential for fishes in the STA to have a greater impact on nutrient cycling than may be expected in other regions.

Current work quantifying the tissue stoichiometry of both small-bodied and large-bodied fishes will help to estimate the contribution of fishes to the total nutrient budget and evaluate their potential to serve as nutrient sinks. Moreover, nutrient excretion trials being conducted to quantify mass-specific P and N excretion rates by fishes will aid to estimate the role of fishes in water column nutrient recycling. Lastly, starting in July 2017, field enclosure experiments will be conducted to estimate the effects of large-bodied fishes on nutrient translocation resulting from resuspension of sediments via bioturbation.

Table 7. Electrofishing mean CPUE of fishes captured in the study sites during February, April, and October 2016 sampling. Sampling efforts consisted of between 12 and 24 5-minute transects per STA sampling event.

Common Name	Colombilio Nome		CPUE			
Common Name	Scientific Name	STA-2	STA-1E	STA-1W		
Brown Bullhead	Ameiurus nebulosu	0.07	0.06	0.06		
Bowfin	Amia calva	0.27	0.24	0.18		
Mayan Cichlid	Cichlasoma urophthalmus	0.26	0.53	0.31		
Walking Catfish	Clarias batrachus	0.02	0.04	0.03		
Gizzard Shad	Dorosoma cepedianum	0	0.2	0.03		
Lake Chubsucker	Erimyzon sucetta	0.04	0.19	0.01		
Seminole Killifish	Fundulus seminolis	0.48	1.94	1.22		
Brown Hoplo	Hoplosternum litorale	0.04	0.14	0		
Florida Gar	Lepisosteus platyrhincus	0.55	0.88	1.46		
Warmouth	Lepomis gulosus	0.18	0.43	0.15		
Bluegill	Lepomis macrochirus	1	3.54	1.04		
Redear Sunfish	Lepomis microlophus	0.73	3.52	0.92		
Spotted Sunfish	Lepomis punctatus	0.03	0.07	0.1		
Largemouth Bass	Micropterus salmoides	1.7	1.43	0.47		
Golden Shiner	Notemigonus crysoleucas	0.08	0.23	0.25		
Blue Tilapia	Oreochromis aureus	0.44	2.43	0.69		
Nile Tilapia	Oreochromis niloticus	0.08	0	0		
Black Crappie	Pomoxis nigromaculatus	0	0.04	0.01		
Vermiculated Sailfin Catfish	Pterygoplichthys disjunctivus	0.02	0.48	0.07		
Orinoco Sailfin Catfish	Pterygoplichthys multiradiatus	0.03	0.05	0.03		
Amazon Sailfin Catfish	Pterygoplichthys pardalis	0.02	0.12	0		
	Amphibians					
Greater Siren	Siren lacertina	0.02	0	0.01		

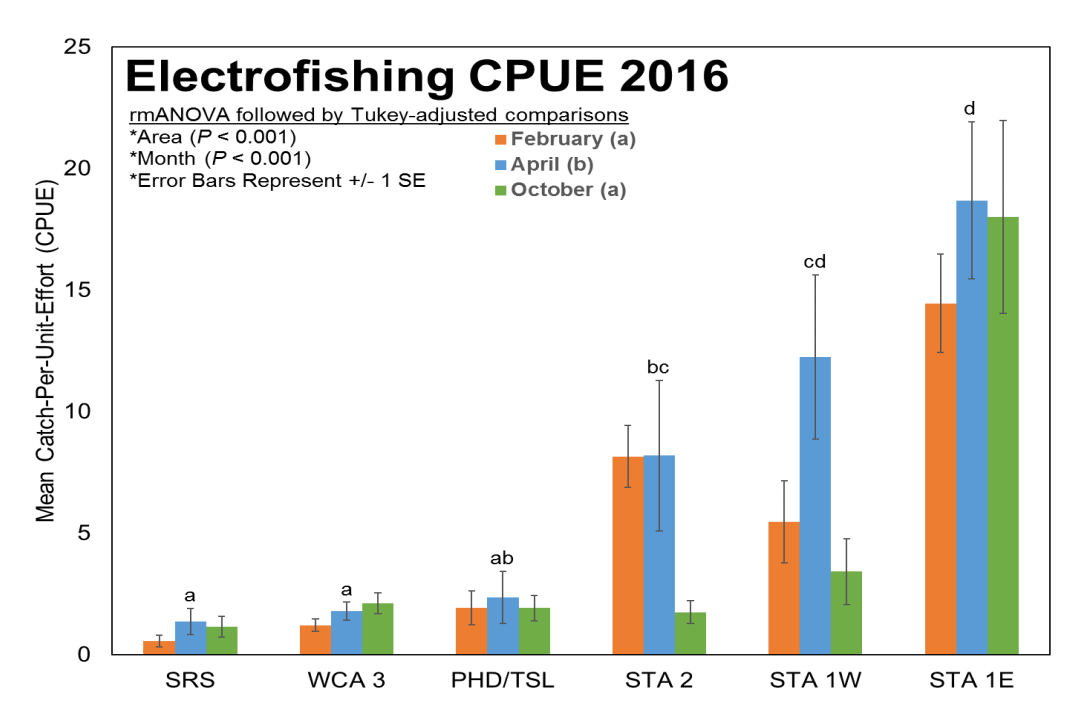


Figure 34. Mean electrofishing CPUE from 5-minute transect samples collected during January/February, March/April, and September/October 2016. Mean discrimination testing results are indicated by the letters above each column with different letters indicating the mean fish CPUEs between the Everglades areas are significantly different ($p \le 0.05$).

LITERATURE CITED

- Ager, L.M. 1971. Fishes of Lake Okeechobee, Florida. *Quarterly Journal of the Florida Academy of Sciences* 34:53-62.
- Bossio, D.A., J.A. Fleck, K.M. Scow and R. Fujii. 2006. Alteration of soil microbial communities and water quality in restored wetlands. *Soil Biology and Biochemistry* 38:1223-1233.
- Briggs, K.T., W.B. Tyler and D.B. Lewis. 1985. Comparison of ship and aerial surveys of birds at sea. *The Journal of Wildlife Management* 49:405-411.
- Chick, J.H., S. Coyne and J.C. Trexler. 1999. Effectiveness of airboat electrofishing for sampling fishes in shallow, vegetated habitats. *North American Journal of Fisheries Management* 19:957-967.
- Childers, D.L., R.F. Doren, R. Jones, G.B. Noe, M. Rugge and L.J. Scinto. 2003. Decadal change in vegetation and soil phosphorus pattern across the Everglades landscape. *Journal of Environmental Quality* 32:344-362.
- DBE. 2015. Field and Supplemental Laboratory Support for Evaluating Phosphorus Sources, Flux, and Transformation Processes in the Stormwater Treatment Areas Project Work Plan. Prepared by DB Environmental, Inc. under Agreement 4600003029-WO01 for South Florida Water Management District, West Palm Beach, FL. Submitted April 15, 2015.
- DBE. 2016. Field and Supplemental Laboratory Support for Evaluating Phosphorus Sources, Flux, and Transformation Processes in the Stormwater Treatment Areas Annual Report. Prepared by DB Environmental, Inc. under Agreement 4600003029-WO01 for South Florida Water Management District, West Palm Beach, FL. Submitted June 21, 2016.

- DBE. 2017. Field and Supplemental Laboratory Support for Evaluating Phosphorus Sources, Flux, and Transformation Processes in the Stormwater Treatment Areas Annual Report. Prepared by DB Environmental, Inc. under Agreement 4600003029-WO01 for South Florida Water Management District, West Palm Beach, FL. Submitted June 2, 2017.
- DeBusk, W., S. Newman and K. Reddy. 2001. Spatio—temporal patterns of soil phosphorus enrichment in Everglades Water Conservation Area 2A. *Journal of Environmental Quality* 30:1438-1446.
- Dorn, N.J. 2013. Consumptive effects of crayfish limit snail populations. *Freshwater Science* 32:1298-1308.
- Dorn, N.J., R. Urgelles and J.C. Trexler. 2005. Evaluating active and passive sampling methods to quantify crayfish density in a freshwater wetland. *Journal of the North American Benthological Society* 24:346-356.
- Doughty, C.E., J. Roman, S. Faurby, A. Wolf, A. Haque, E.S. Bakker, Y. Malhi, J.B. Dunning and J.C. Svenning. 2016. Global nutrient transport in a world of giants. *Proceedings of the National Academy of Sciences* 113:868-873.
- Dunne, E.J., M.W. Clark, J. Mitchell, J.W. Jawitz and K.R. Reddy. 2010. Soil phosphorus flux from emergent marsh wetlands and surrounding grazed pasture uplands. *Ecological Engineering* 36(10):1392-1400.
- Fisher, M.M. and K.R. Reddy. 2001. Phosphorus flux from wetland soils affected by long-term nutrient loading. *Journal of Environmental Quality* 30(1):261-271.
- Jordan, F., S. Coyne and J.C. Trexler. 1997. Sampling fishes in vegetated habitats: Effects of habitat structure on sampling characteristics of the 1-m² throw trap. *Transactions of the American Fisheries Society* 126:1012-1020.
- Julian, P. and S. Hill. 2012. A.R.M. Loxahatchee National Wildlife Refuge Total Phosphorus Outlier Analysis and Proposed Alternative Screening Criterion: Distribution Independent Outlier Analysis. Presented to the Everglades Technical Oversight Committee on May 30, 2012. Available from the South Florida Water Management District, West Palm Beach, FL.
- Juston, J.M., T.A. DeBusk, K.A. Grace and S.D. Jackson. 2013. A model of phosphorus cycling to explore the role of biomass turnover in submerged aquatic vegetation wetlands for Everglades restoration. *Ecological Modelling* 251:135-149.
- Kadlec, R.H. and S.D. Wallace. 2009. Treatment Wetlands, Second Edition. CRC Press, Boca Raton, FL.
- Kear, J. 2005. *Ducks, Geese and Swans: Species Accounts (*Cairina to Mergus), *Volume 2*. Oxford University Press, Oxford, UK.
- Kellog, C.M. and N.J. Dorn. 2012. Consumptive effects of fish reduce wetland crayfish recruitment and drive species turnover. *Oecologia* 168:1111-1121.
- Loftus, W. F. and J. A. Kushlan. 1987. Freshwater fishes of southern Florida. *Bulletin of the Florida State Museum*, Biological Science Series 31:147-344.
- SFWMD. 2012. Restoration Strategies Regional Water Quality Plan. South Florida Water Management District, West Palm Beach, FL. April 27, 2012. Available on line at https://www.sfwmd.gov/sites/default/files/documents/rs waterquality plan 042712 final.pdf.
- SFWMD. 2013. Science Plan for the Everglades Stormwater Treatment Areas. South Florida Water Management District, West Palm Beach, FL. June 2013. Available online at https://www.sfwmd.gov/sites/default/files/documents/rs scienceplan 060713 final.pdf.

- Thomas, L., S.T. Buckland, E.A. Rexstad, J.L. Laake, S. Strindberg, S.L. Hedley, J.R. Bishop, T.A. Marques and K.P. Burnham. 2010. Distance software: Design and analysis of distance sampling surveys for estimating population size. *Journal of Applied Ecology* 47:5-14.
- Vanni, M.J. 2002. Nutrient cycling by animals in freshwater ecosystems. *Annual Review of Ecology and Systematics* 33:341-370.
- Vanni, M.J., A.M. Bowling, E.M. Dickman, R.S. Hale, K.A. Higgins, M.J. Horgan, L.B. Knoll, W.H. Renwick and R.A. Stein. 2006. Nutrient cycling by fish supports relatively more primary production as lake productivity increases. *Ecology* 87:1696-1709.